ANL/NSE-18/7

Advanced Model Developments in SAM for Thermal Stratification Analysis during Reactor Transients

Nuclear Science and Engineering Division

About Argonne National Laboratory
Argonne is a U.S. Department of Energy laboratory managed by UChicago Argonne, LLC under contract DE-AC02-06CH11357. The Laboratory's main facility is outside Chicago, at 9700 South Cass Avenue, Argonne, Illinois 60439. For information about Argonne and its pioneering science and technology programs, see www.anl.gov.

ANL/NSE-18/7

Advanced Model Developments in SAM for Thermal Stratification Analysis

prepared by
Rui Hu, Yangmo Zhu, Adam Kraus
Nuclear Science and Engineering Division, Argonne National Laboratory

September 2018

EXECUTIVE SUMMARY

Mixing, thermal-stratification, and mass transport phenomena in large pools or enclosures play major roles for the safety of reactor systems. Depending on the fidelity requirement and computational resources, various modeling methods, from the 0-D perfect mixing model to 3-D Computational Fluid Dynamics (CFD) models, are available. Each is associated with its own advantages and shortcomings. It is very desirable to develop an advanced and efficient thermal mixing and stratification modeling capability embedded in a modern system analysis code to improve the accuracy of reactor safety analyses and to reduce modeling uncertainties.

An advanced system analysis tool, SAM, is being developed at Argonne National Laboratory for advanced non-LWR reactor safety analysis, under the support of U.S. Department of Energy (DOE) Nuclear Energy Advanced Modeling and Simulation (NEAMS) program. It aims to provide fast-running, modest-fidelity, whole-plant transient analyses capabilities, which are essential for fast turnaround design scoping and engineering analyses of advanced reactor concepts. While SAM is being developed as a system-level modeling and simulation tool, advanced modeling techniques are under development to tackle the issue of thermal mixing and stratification modeling in large enclosures of reactor systems during transients.

This report summarizes the recent progress on the reduced-order flow model developments in SAM for thermal stratification and mixing modeling. Three modeling approaches are pursued. The first one is similar to the approach used in conventional system codes which models a large enclosure with multiple zero dimensional volumes. The second approach is based on one-dimensional fluid models with additional terms accounting for the thermal mixing from both macroscopic flow circulations and microscopic turbulent mixing. The third approach is based on three-dimensional coarse-grid CFD approach, in which the full three-dimensional fluid conservation equations are modeled with closure models to account for the effects of turbulence.

The SAM 0-D modeling approach is based on the concept that the large enclosure can be divided into a number of sub-regions (multiple 0-D volumes), separated by horizontal interfaces. The feasibility of the multiple 0-D volume modeling approach was tested using the EBR-II loss-of-heat-sink test BOP-302R. Focused on the thermal-hydraulics responses of the system throughout the transients in which the reactor power history was specified in the input model, very good agreement was found among the code simulations and the test results. The high- and low-pressure inlet plena temperatures from the SAM simulation agreed very well with the test for both the initial heat up rates and the later pseudo-equilibrium states. It is thus demonstrated that it is feasible to account for the effects of thermal stratification in the cold pool by a simple multiple 0-D volume cold pool model. The simulation results were highly dependent on the assumption of the mixing flow rates between the upper and lower cold pools. Therefore, companion CFD simulations are suggested to develop correlations between the mixing flow rates at horizontal cross planes and the lumped sub-volume parameters for each large enclosure if it would be modeled in SAM with the multiple 0-D volume approach.

The SAM 1-D modeling approach is based on similar concept of multiple 0-D volume approach that the large enclosure can be divided into arbitrary number of sub-volumes, separated by horizontal interfaces. However, the one-dimensional fluid conservation equations

are used. The inter-volume or inter-element energy exchange can be modeled through both advection and mixing flow. Note that additional models for the mixing velocity are needed, for which the high-fidelity CFD simulations using LES and uRANS can assist in the closure model developments. A new governing (conservation) equation is introduced in our work for the mixing velocity. Recognizing three major contributions of the mixing flow, including local flow velocity, geometry, and the buoyancy effects, two parameters C_{gb} and C_{gv} are introduced in the mixing velocity equation.

The 1-D axial mixing model was first verified with two simple 1-D channel flow test cases, including the inlet temperature sharp change case and inlet temperature oscillation (following a sinusoidal function) case. Various modeling approaches and modeling parameters are tested for both test cases. The impacts of flow mixing were clearly observed in the two test cases. To verify the applicability of the developed 1-D axial mixing model, another test problem was developed based on the geometry and operating conditions of the upper plenum in the Advanced Burner Test Reactor (ABTR) design. Transient CFD simulations of a stand-alone tank model were also performed to provide the reference solutions. With increasing complexities of SAM models (but still in 1D and 0D) to represent the tank flow, the SAM simulation results became similar to the reference CFD simulation results. If the upper part of the tank (above the outlet pipe) was neglected in the SAM models, the outlet temperature responses would be far away from the reference CFD simulation results. If the upper tank is modeled, the SAM simulation results are much closer to the CFD results. As seen from the CFD simulation results, the upper part of the tank was not stagnant during the transient and strongly participated in the flow circulation and mixing in the tank. This preliminary demonstration case provides us confidence that the 1D axial mixing model could simulate the macroscopic behavior in SFR pools during transients with both accuracy and efficiency.

A reduced-order three-dimensional module is also under development to model the multi-dimensional flow and thermal mixing and stratification in large enclosures of reactor systems. For computationally efficient modeling capabilities, the key modeling approaches include: 1) solving the full 3-D fluid conservation equations; 2) using only coarse computational meshes; and 3) excluding turbulence modeling. The framework of a 3-D FEM flow model has been developed and implemented in SAM. Closure models (mainly turbulence viscosity) in the 3-D flow model is being developed to account for the effects of turbulence and the use of a coarse mesh in momentum and energy transport. A data-driven closure model (turbulence viscosity) development framework has been developed to leverage machine learning (ML) technique to establish a surrogate model to replace the turbulence modeling in traditional CFD code. The framework and workflow is tested with a transient flow in a large enclosure. This test case aims to simulate a transient scenario mimicking the flow in an SFR upper plenum during a postulated loss-of-flow transient. With only 4.2% of the total data used as training data, the prediction accuracy of the trained ML model is very high, i.e. 86.34% of the predictions had errors of less than 5e-5.

All three modeling approaches have been pursued and implemented in SAM, as all showed promise to model the thermal mixing and stratification during reactor transient. Additional closure model development is needed for all three approaches. It is thus recommended to perform companion high-fidelity CFD simulations to assist in the model development for any specific designs.

Table of Contents

LIST OF FIGURES

LIST OF TABLES

1 Introduction

Mixing, thermal-stratification, and mass transport phenomena in large pools or enclosures play major roles for the safety of reactor systems. Such phenomena include the cold and hot pool mixing in pool-type Sodium-cooled Fast Reactors (SFR), reactor cavity cooling system behavior in High Temperature Gas-cooled Reactors (HTGR), passive containment cooling in advanced light-water reactors (such as AP1000), and thermal-stratification in BWR suppression pools. It is very important to accurately predict pool temperature and density distributions for both design optimizations and safety analyses of these reactor systems. However, the individual transport mechanisms governing mixing are characterized by time and length scales that can differ by orders of magnitude. Large volumes and complex interactions of different flow and thermal structures make the analysis of mixing in a large enclosure a very challenging task (intractable by analytic means and extremely demanding from a computational standpoint). Due to these reasons, experimental efforts [1-3] including large facilities like PANDA [3,4] have been continuously investigating these phenomena over the past three decades.

Depending on the fidelity requirement and computational resources, 0-D steady state models, 0-D lumped parameter based transient models, 1-D physical-based models, and 3-D Computational Fluid Dynamics (CFD) models are available. A good overview on major modeling methods of thermal mixing and stratification phenomena and their advantages and limits can be found in Reference [5].

Current major system analysis or severe accident analysis codes (such as SAS4A/SASSYS-1[6], RELAP5[7], CATHRE[8], and MELCOR[9]) either have no models or only 0-D models for thermal mixing and stratification in large enclosures. The lack of general thermal mixing and stratification models in those codes severely limits their application and accuracy for safety analysis, especially for reactors relying on natural circulation for long-term cooling.

For example, the SAS4A/SASSYS-1 code developed by Argonne National Laboratory ("Argonne"), one of the major SFR system analysis codes, provides lumped-volume-based 0-D models that can only give very approximate results and can only handle simple cases with one mixing source. The models were derived according to simulant experiments for specific SFR upper plenum design configurations. Depending on the momentum and buoyancy of the outlet flow from the reactor core, well mixed case, two-zone with a negative buoyant jet case, two-zone with a positive buoyant jet case, and even more complex three-zone cases may form. The total jet entrainment, zone interface location, and average temperatures in each zone can be estimated by empirical correlations. Since the methods are based on scaled experimental data, using those models for SFR designs with different hot/cold pool configurations tends to result in large uncertainties.

Scaling analyses for prediction of thermal stratification and mixing in pools and in large interconnected enclosures were developed and applied by Peterson and coworkers at UC Berkeley [10,11]. A 1-D simulation code BMIX/BMIX++ was also developed to simulate stratification development in stably stratified conditions [12]. The ambient fluid volume is represented by 1-D transient partial differential equations, and substructures such as free or wall jets are modeled with 1-D integral models. This allows very large reductions in computational effort compared to 3-D CFD modeling. It was validated against a number of benchmark problems [13,14]. However, BMIX++ cannot model the transition cases where the fully stratified ambient or well-mixed

ambient assumptions break down. For a transient where initially stratified pool is gradually mixed, it cannot help to infer about the time scale for such mixing processes.

Reynolds-Averaged Navier-Stokes (RANS) based CFD approaches are less expensive than higher fidelity Large Eddy Simulations (LES), and has been applied in SFR upper plenum simulation with very detailed geometric modeling of major structures [15]. However, it is still computationally overwhelming for long-transient, complex-flow simulations in engineering applications, particularly when sensitivity/uncertainty analysis is needed for design optimizations and safety analyses. Multi-scale modeling approaches (achieved by coupling 1-D system and 3-D CFD codes) has been tried to simulate large and complex domains by modeling the large volume with a CFD code and the rest of the system with a system code [16,17]. This methodology can provide detailed information only where needed while providing system level information in the rest of the domain. However, coupling different codes employing different solver routines and operating at different spatial and temporal scales remains a challenge. A notable fundamental problem is that a reliable and accurate coupling scheme is largely missing in the treatment of momentum and energy exchange at the boundary between the CFD model and the system model. It is very desirable to have an advanced and efficient thermal mixing and stratification modeling capability embedded in a system analysis code to improve the accuracy of reactor safety analyses and to reduce modeling uncertainties.

An advanced system analysis tool, SAM [18], is being developed at Argonne National Laboratory for advanced non-LWR reactor safety analysis. It aims to provide fast-running, modest-fidelity, whole-plant transient analyses capabilities, which are essential for fast turnaround design scoping and engineering analyses of advanced reactor concepts. While SAM is being developed as a system-level modeling and simulation tool [19,20], advanced modeling techniques including a reduced-order three-dimensional module are under development to tackle the issue of thermal mixing and stratification modeling in large enclosures of reactor systems during transients.

This report summarizes the recent progress on the reduced-order flow model developments in SAM for thermal stratification and mixing modeling. Three different modeling approaches are pursued. The first one is similar to the approach used in conventional system codes which models a large enclosure with multiple zero dimensional volumes. The second approach is based on one-dimensional fluid models with additional terms accounting for the thermal mixing from both macroscopic flow circulations and microscopic turbulent mixing. The third approach is based on three-dimensional coarse-grid CFD approach, in which the full three-dimensional fluid conservation equations are modeled with closure models to account for the effects of turbulence. The technical basis of the three modeling approaches are discussed first, followed by some initial demonstration simulations and validation tests. The details of each modeling approach are presented in Chapter 3 through 5, respectively.

2 SAM Overview

The System Analysis Module (SAM) [18] is an advanced system analysis tool being developed at Argonne National Laboratory under the support of U.S. Department of Energy (DOE) Nuclear Energy Advanced Modeling and Simulation (NEAMS) program. It aims to be a modern system analysis code, which takes advantage of the advancements software design, numerical methods, and physical models over the past two decades. SAM focuses on modeling advanced reactor concepts such as SFRs (sodium fast reactors), LFRs (lead-cooled fast reactors), and FHRs (fluoride-salt-cooled high temperature reactors) or MSRs (molten salt reactors). These advanced concepts are distinguished from light-water reactors (LWR) in their use of single-phase, low-pressure, high-temperature, and low Prandtl number (sodium and lead) coolants. This simple yet fundamental change has significant impacts on core and plant design, the types of materials used, component design and operation, fuel behavior, and the significance of the fundamental physics in play during transient plant simulations.

SAM is aimed to solve the tightly-coupled physical phenomena including heat generation, heat transfer, fluid dynamics, and thermal-mechanical response in reactor structures, systems and components in a fully-coupled fashion but with reduced-order modeling approaches to facilitate rapid turn-around for design and safety optimization studies. As a new code development, the initial effort focused on developing modeling and simulation capabilities of the heat transfer and single-phase fluid dynamics responses in reactor systems. This Chapter discusses goals and objectives, software structure, the governing theory, as well as current capabilities of the code. In the coming years, the SAM code will continuously mature as a modern system analysis tool for advanced (non-LWR) reactor design optimization, safety analyses, and licensing support.

2.1 Ultimate Goals and Objectives

The ultimate goal of SAM is to be used in advanced reactor safety analysis for design optimization and licensing support. The important physical phenomena and processes that may occur in reactor systems, structures, and components shall be of interest during reactor transients including Anticipated Operational Occurrence (AOO), Design Basis Accident (DBA), and additional postulated accidents but not including severe accidents. Typical reactor transients include: loss of coolant accidents, loss of flow events, excessive heat transfer events, loss of heat transfer events, reactivity and core power distribution events, increase in reactor coolant inventory events, and anticipated transients without scram (ATWS).

As a modern system analysis code, SAM is also envisioned to expand beyond the traditional system analysis code to enable multi-dimensional flow analysis, containment analysis, and source term analysis, either through reduced-order modeling in SAM or via coupling with other simulation tools. Additionally, the regulatory processes in the United States is being evolved to a risk-informed approach that is based on first understanding the best-estimate behavior of the fuel, the reactor, the reactor coolant system, the engineered safeguards, the balance of plant, operator actions, and all of the possible interactions among these elements. To enable this paradigm, an advanced system analysis code such as SAM must be able to model the integrated response of all of these physical systems and considerations to obtain a best-estimate simulation that includes both validation and uncertainty quantification.

The SAM code is aimed to provide improved-fidelity simulations of transients or accidents in an advanced non-LWR, including three-dimension resolutions as needed or desired. This will

encompass the fuel rod, the fuel assembly, the reactor, the primary and intermediate heat transport system, the balance-of-plant, the containment. Multi-dimension, multi-scale, and multi-physics effects will be captured via coupling with other simulation tools, and computational accuracy and efficiency will be state-of-the-art. Uncertainty quantification will be integrated into SAM numerical simulations. Legacy issues such as numerical diffusion and stability in traditional system codes will be addressed and the code will attract broad use across the nuclear energy community based on its performance and many advantages relative to the legacy codes. The integrated architecture will provide a robust toolset for decision making with full consideration of the various disciplines and technologies affecting an issue.

2.2 Software Structure

SAM is being developed as a system-level modeling and simulation tool with higher fidelity (compared to existing system analysis tools), and with well-defined and validated simulation capabilities for advanced reactor systems. It provides fast-running, modest-fidelity, whole-plant transient analyses capabilities. To fulfill the code development, SAM utilizes the object-oriented application framework MOOSE [21] and its underlying meshing and finite-element library libMesh [22] and linear and non-linear solvers PETSc [23], to leverage the available advanced software environments and numerical methods. The high-order spatial discretization schemes, fully implicit and high-order time integration schemes, and the advanced solution method (such as the Jacobian-free Newton–Krylov (JFNK) method [24]) are the key aspects in developing an accurate and computationally efficient model in SAM.

The software structure of SAM is illustrated in Figure 2-1. In addition to the fundamental physics modeling of the single-phase fluid flow and heat transfer, SAM incorporates advances in the closure models (such as convective heat transfer correlations) for reactor system analysis developed over the past several decades. A set of Components, which integrate the associated physics modeling in the component, have been developed for friendly user interactions. This component-based modeling strategy is similar to what is implemented in RELAP-7 [25], which is also a MOOSE-based system analysis tool (focused on LWR simulations). A flexible coupling interface has been developed in SAM so that multi-scale, multi-physics modeling capabilities can be achieved by integrating with other higher-fidelity or conventional simulation tools.

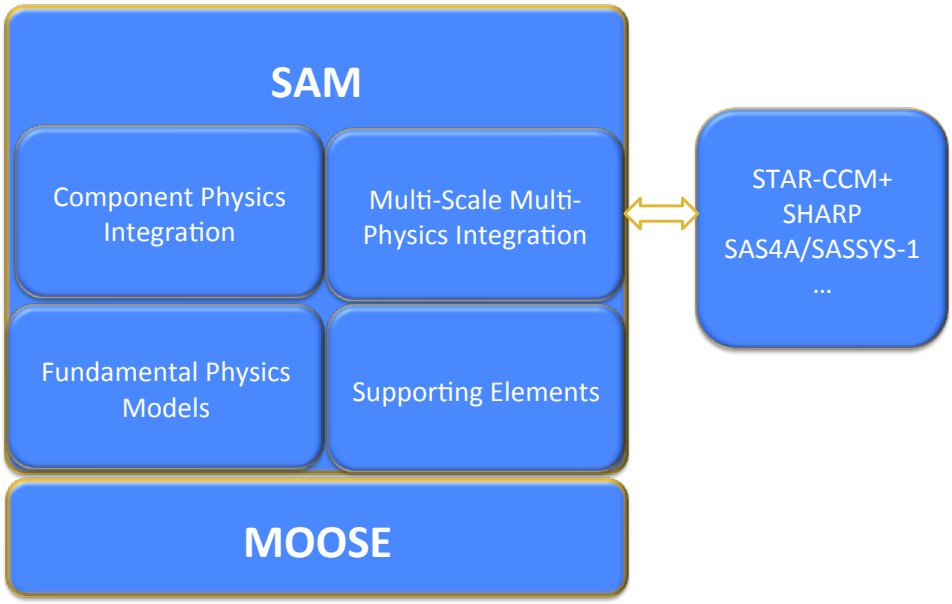

Figure 2-1. SAM Code Structure

2.3 Governing Theory

2.3.1 Fluid dynamics

Fluid dynamics is the main physical model of the SAM code. SAM employs a standard one-dimensional transient model for single-phase incompressible but thermally expandable flow. The governing equations consist of the continuity equation, momentum equation, and energy equations. A three-dimensional module is also under development to model the multi-dimensional flow and thermal stratification in the upper plenum or the cold pool of an SFR. Additionally, a subchannel module will be developed for fuel assembly modeling.

2.3.2 Heat transfer

Heat structures model heat conduction inside solids and permit the modeling of heat transfer at interfaces between solid and fluid components. Heat structures are represented by one-dimensional or two-dimensional heat conduction in Cartesian or cylindrical coordinates. Temperature-dependent thermal conductivities and volumetric heat capacities can be provided in tabular or functional form. Heat structures can be used to simulate the temperature distributions in solid components such as fuel pins or plates, heat exchanger tubes, and pipe and vessel walls, as well as to calculate the heat flux conditions for fluid components. Flexible conjugate heat transfer and thermal radiation modeling capabilities are also implemented in SAM.

2.3.3 Closure Models

The fluid equation of state (EOS) model is required to complete the governing flow equations, which are based on the primitive variable formulation; therefore, the dependency of fluid properties and their partial derivatives on the state variables (pressure and temperature) are implemented in the EOS model. Some fluid properties, such as sodium, air, salts like FLiBe and

FLiNaK, have been implemented in SAM. Empirical correlations for friction factor and convective heat transfer coefficient are also required in SAM because of its one-dimension approximation of the flow field. The friction and heat transfer coefficients are dependent on flow geometries as well as operating conditions during the transient.

2.3.4 Mass transport model development

The mass transport modeling capability is needed to model sources and transport of particles for a number of applications, such as tritium transport, delayed neutron precursor drift, radioactive isotope transport for molten salt fueled/cooled systems. A general passive scalar transport model has been implemented in SAM, and it can be used to track any number of species carried by the fluid flow.

2.3.5 Reactor Kinetics model development

SAM employs a built-in point kinetics model, including reactivity feedback and decay heat modeling. Since this development is a relatively new effort, enhancements of the reactivity feedback modeling are also needed to include additional reactivity feedback mechanisms due to thermal expansion effects.

2.3.6 Numerical Methods

SAM is a finite-element-method based code. The "weak forms" of the governing equations are implemented in SAM. It uses the Jacobian-Free Newton Krylov (JFNK) solution method to solve the equation system. The JFNK method uses a multi-level approach, with outer Newton's iterations (nonlinear solver) and inner Krylov subspace methods (linear solver), in solving large nonlinear systems. The concept of 'Jacobian-free' is proposed, because deriving and assembling large Jacobian matrices could be difficult and expensive. The JFNK method has become an increasingly popular option for solving large nonlinear equation systems and multi-physics problems, as observed in a number of different disciplines [24]. One feature of JFNK is that all the unknowns are solved simultaneously in a fully coupled fashion. This solution scheme avoids the errors from operator splitting and is especially suitable for conjugate heat transfer problems in which heat conduction in a solid is tightly coupled with fluid flow.

2.4 Overview of Current Capabilities

To develop a system analysis code, numerical methods, mesh management, equations of state, fluid properties, solid material properties, neutronics properties, pressure loss and heat transfer closure laws, and good user input/output interfaces are all indispensable. SAM leverages the MOOSE framework and its dependent libraries to provide JFNK solver schemes, mesh management, and I/O interfaces while focusing on new physics and component model development for advanced reactor systems. The developed physics and component models provide several major modeling features:

1. One-D pipe networks represent general fluid systems such as the reactor coolant loops.
2. Flexible integration of fluid and solid components, able to model complex and generic engineering system. A general liquid flow and solid structure interface model was developed for easier implementation of physics models in the components.

3. A pseudo three-dimensional capability by physically coupling the 1-D or 2-D components in a 3-D layout. For example, the 3-D full-core heat-transfer in an SFR reactor core can be modeled. The heat generated in the fuel rod of one fuel assembly can be transferred to the coolant in the core channel, the duct wall, the inter-assembly gap, and then the adjacent fuel assemblies.
4. Pool-type reactor specific features such as liquid volume level tracking, cover gas dynamics, heat transfer between 0-D pools, fluid heat conduction, etc. These are important features for accurate safety analyses of SFRs or other advanced reactor concepts.
5. A computationally efficient multi-dimensional flow model is under development, mainly for thermal mixing and stratification phenomena in large enclosures for safety analysis. It was noted that an advanced and efficient thermal mixing and stratification modeling capability embedded in a system analysis code is very desirable to improve the accuracy of advanced reactor safety analyses and to reduce modeling uncertainties.
6. A general mass transport capability has been implemented in SAM based on the passive scalar transport. The code can track any number of species carried by the fluid flow for various applications.
7. An infrastructure for coupling with external codes has been developed and demonstrated. The code coupling with STAR-CCM+ [26], SAS4A/SASSYS-1 [27], Nek5000, and BISON [28] have been demonstrated, while the coupling with PRONGHORN, RattleSnake, and PORTEUS codes are being planned.

The examples of SAM simulation results of advanced reactors are shown in Figure 2-2 to Figure 2-4 for SFR, FHR, and MSR.

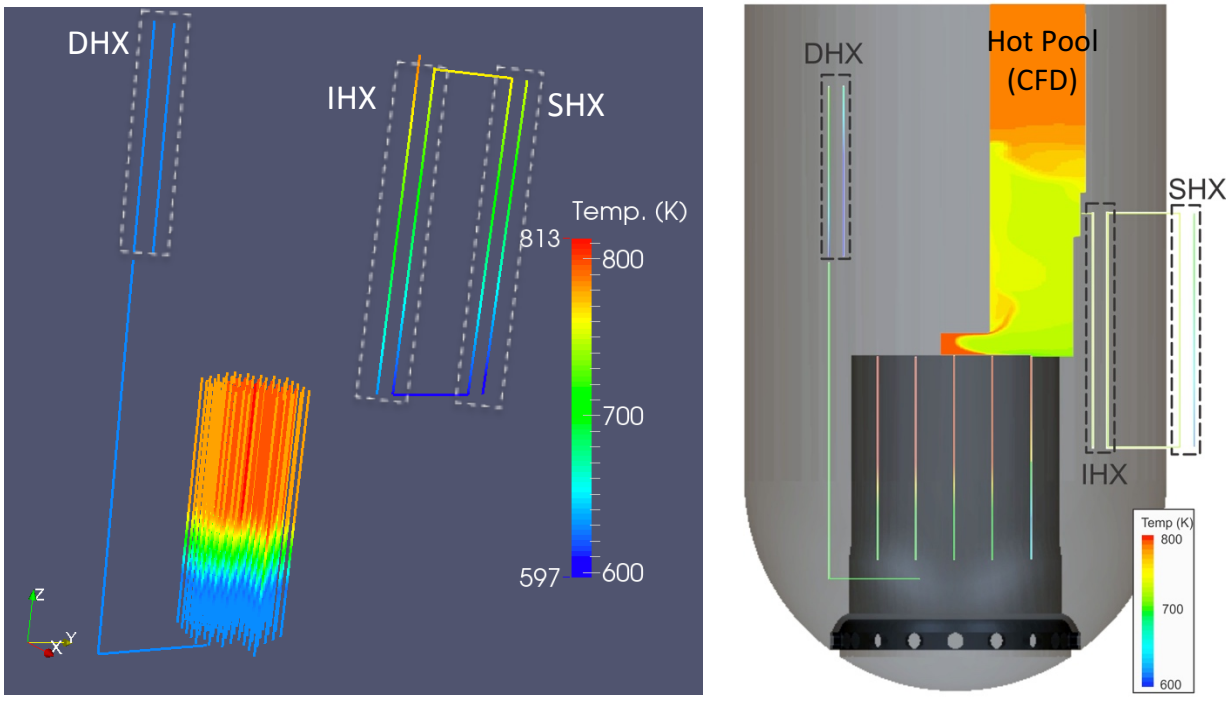

(a) SAM model with 61 core channels (b) Coupled SAM and CFD code simulation

Figure 2-2. SAM simulation results of an SFR [26]

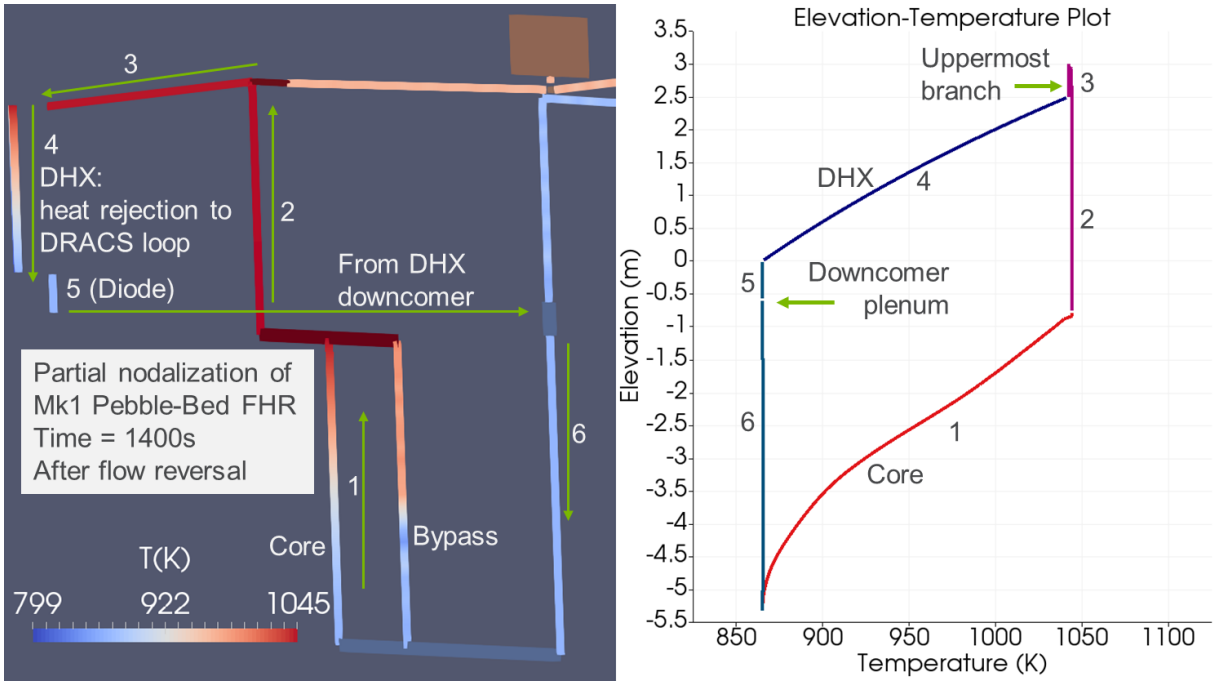

Figure 2-3. SAM simulation results of an FHR [29]

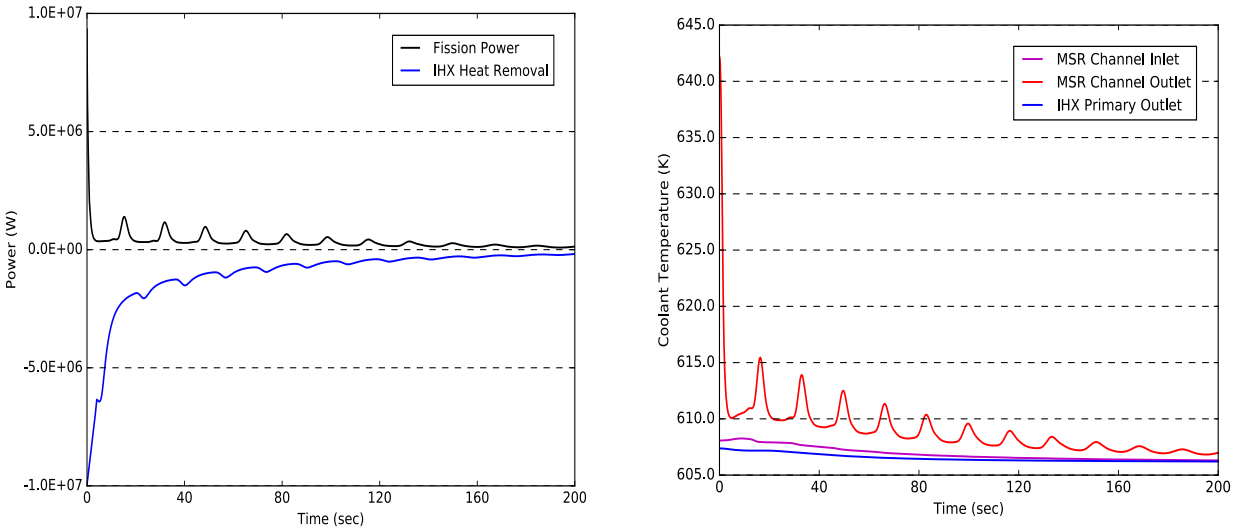

(a) Power

Figure 2-4. SAM simulation results of a simple MSR primary loop during a postulated loss-of-flow transient [30]

3 0-D Volume Modeling Approach

3.1 0-D Mixing Model

As discussed in Chapter 1, current major system analysis codes only have 0-D models for thermal mixing and stratification in large enclosures. For example, SAS4A/SASSYS-1 code provides lumped-volume-based 0-D models that can give very approximate results and can only handle simple cases with one mixing source. The basic concept is based on that the lumped enclosure is made up of a small number of distinct temperature regions, separated by horizontal interfaces. Depending on the momentum and buoyancy of the jet flow into the large enclosures, well mixed case, two-zone with a negative buoyant jet case, two-zone with a positive buoyant jet case, and even more complex three-zone cases may form. The total jet entrainment, zone interface location, and average temperatures in each zone can be estimated by empirical correlations. Since the methods are based on scaled experimental data, using those models for SFR designs with different hot/cold pool configurations tends to result in large uncertainties.

A general multiple 0-D volume modeling approach is also implemented in SAM, as shown in Figure 3-1. A large enclosure is modeled by a number of 0-D average volumes, where inter-volume directional flow and mixing flows are allowed.

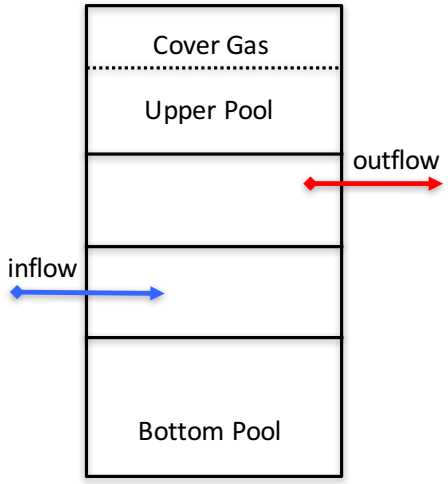

Figure 3-1. Multi-Volume 0-D Pool Model.

A special SAM Component, *StagnantVolume,* has been implemented to models a stagnant liquid volume, which has no connections to 1-D fluid components but is allowed to connect to a 0-D volume or 1-D or 2-D heat structures for heat transfer. It is assumed that there is no net mass transfer between *StagnantVolume* and the connecting 0-D volumes. The governing equation of the energy conservation for the *StagnantVolume* can be given as:

$$\frac{d(\rho V H)}{dt} + \sum_{i=1}^{n} \dot{Q}_i = 0 \qquad (3\text{-}1)$$

In which,

ρ: average density of the *StagnantVolume* component;
V: total volume of the component;

H: average enthalpy of the volume component.
t: time;
n: the number of coupling heat transfer components;
$\dot{Q}$: heat transfer with coupled heat structures or 0-D volumes;

For convective heat transfer with heat structures,

$$\dot{Q} = \int h_{conv}(T_w - T_{vol})\, dA\,. \tag{3-2}$$

In which,

h_{conv}: convective heat transfer coefficient;
T_w: structure wall temperature;
T_{vol}: volume temperature.

For heat transfer with other 0-D volumes through thermal mixing,

$$\dot{Q} = \dot{m}_{mix}\Delta H. \tag{3-3}$$

In which,

$\dot{m}_{mix}$: the effective mixing flow between 0-D volumes;
ΔH: enthalpy differences between 0-D volumes.

3.2 Demonstration Case

The feasibility of the multiple 0-D volume modeling approach was tested using an available EBR-II test BOP-302R. BOP-302R was a loss of heat sink test where the intermediate sodium pump was tripped without scramming the control rods or tripping the primary pumps. This test was driven by increasing core inlet temperatures, which were a result of the diminished IHX heat rejection due to the lower intermediate sodium flow rates. Strong thermal stratification is expected in the primary vessel (cold pool), where the IHX outlet and the pump inlets are located in the upper part of the vessel.

To correctly predict the core inlet temperature, the thermal stratification in the cold pool needs to be properly considered. This is accounted for in the SAM simulation with a two-volume pool model, in which the upper volume connects with the main primary pumps and the IHX, and the lower volume is stagnant but the mixing flow with the upper volume and the convective heat transfer with the immersed piping walls are considered. Similar modeling approaches were also adopted in the SAS4A/SASSYS-1 model. In the SAM BOP-302R simulation, the mixing flow between the upper and lower cold pool is assumed to be 50% of the primary core flow rate.

Simulation results of the BOP-302R test are shown in Figure 3-2 through Figure 3-4. Very good agreement was found among the SAM and SAS simulations and the test results. More details on the SAM model and simulation results can be found an earlier paper [31].

SAM predictions of the plena temperatures during BOP-302R test are shown in Figure 3-2. SAM predictions of plena temperatures during BOP-302R test. The upper cold pool temperature increases rapidly at the beginning of the transient due to the loss-of-cooling in the IHX. As the primary loop coolant flow rate is largely unchanged throughout the transient, the core outlet plenum temperature drops with the decrease of the core power. As the IHX primary outlet temperature decreases and the continuous mixing between the upper and lower cold pool, the upper cold pool temperature decreases eventually after reaching a peak. The temperature responses in

the high- and low-pressure core inlet plena are similar to the upper cold pool, and the temperature at the low-pressure inlet plenum is slightly lower due to the heat loss to the lower cold pool through the long piping. The lower cold pool temperature response is much slower compared to other volumes, as it does not directly participate in the primary coolant flow loop. Eventually all plena temperatures became very close to each other as the lower cold pool was heated up.

The comparisons of high-pressure inlet plena temperatures from the SAM and SAS simulations and the test results are shown in Figure 3-3. Very good agreement was achieved for both the initial heat up rates and the later pseudo-equilibrium states. It is demonstrated that the thermal stratification in the cold pool during the test can be modeled with a relatively simple multiple 0-D volume model. Note that the mixing flow rates between 0-D volumes are crucial to accurately model the heat transfer between 0-D volumes, and the mixing flow rates can be derived from uRANS-based CFD simulations.

The core outlet temperature of the driver fuel subassembly 6C4 is shown in Figure 3-4. The transient trends among the experiment and the two simulations are very similar, but the initial increase of core outlet temperature was not observed in the test results. It is suspected again that the mixing between the subassembly 6C4 and the adjacent low power subassemblies reduced its outlet temperature measurement in the test. Very similar results are found between the SAM and SAS simulations.

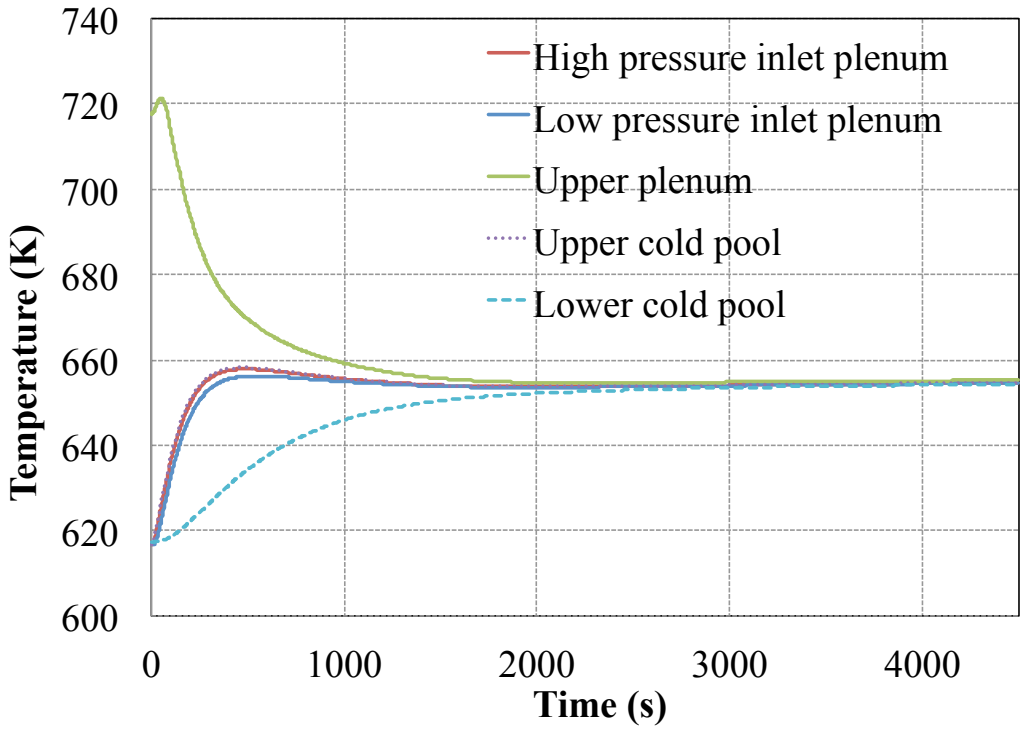

Figure 3-2. SAM predictions of plena temperatures during BOP-302R test

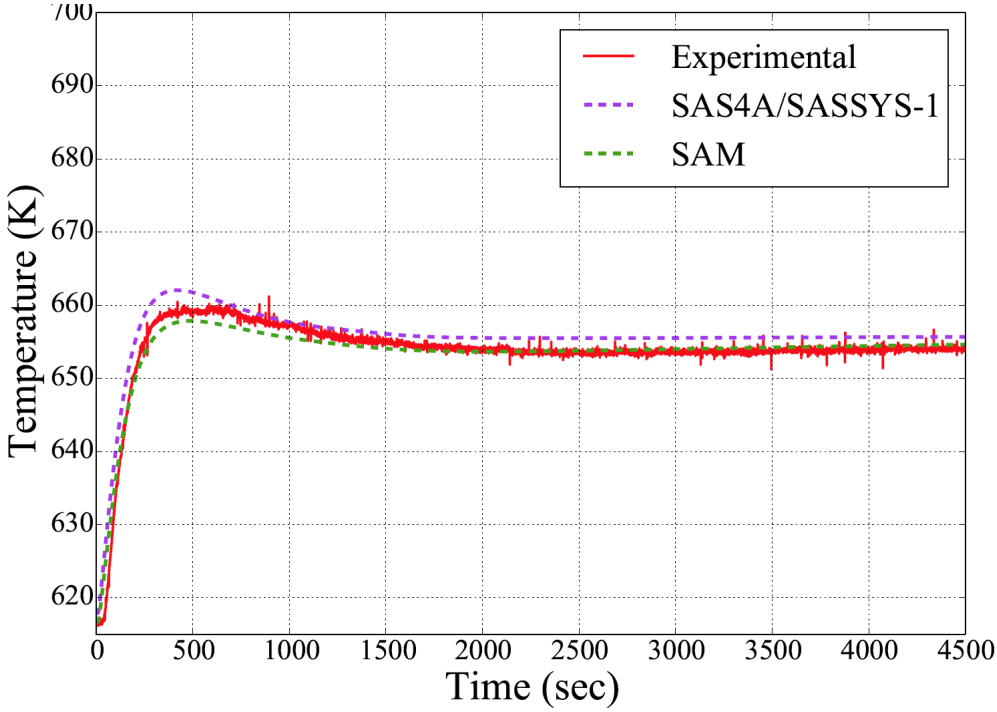

Figure 3-3. High-pressure inlet plenum temperature during BOP-302R test

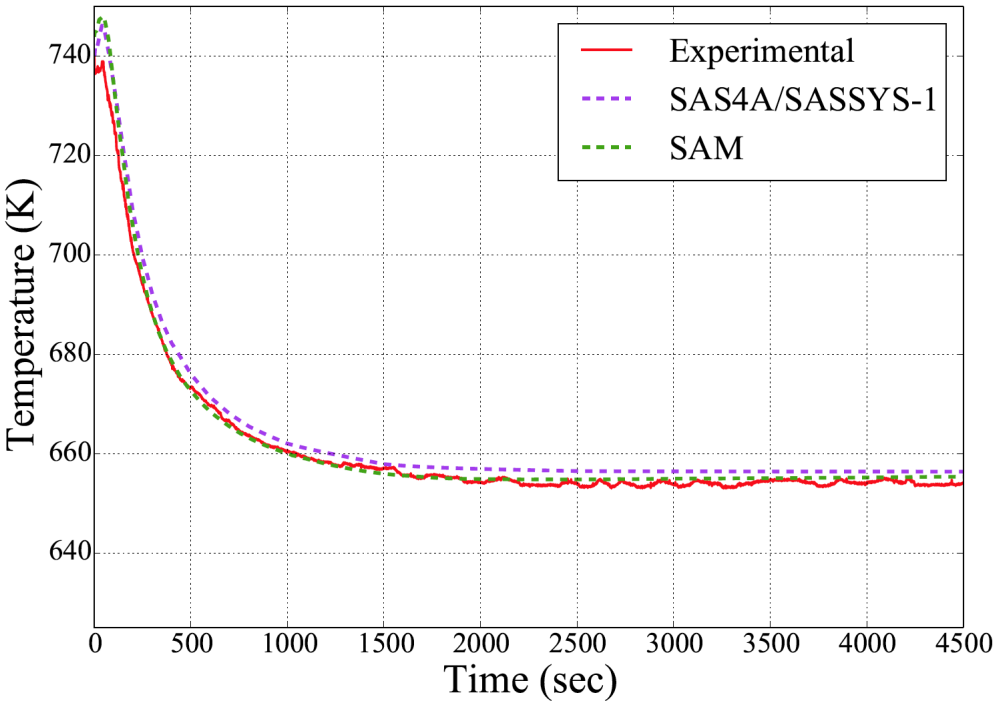

Figure 3-4. Subassembly 6C4 outlet temperature during BOP-302R test

4 One-D Modeling Approach

4.1 1D Axial Mixing Model

The SAM 1-D modeling approach is based on similar concept of multiple 0-D volume approach that the large enclosure can be divided into arbitrary number of sub-volumes, separated by horizontal interfaces. The inter-volume energy exchange can be modeled by both advection and flow mixing. The one-dimensional fluid conservation equations are used for the 1D axial mixing model. To consider the flow mixing, the energy conservation equation can be written as:

$$\frac{\partial(\rho H)}{\partial t}+\frac{\partial((\rho u+G_{mix})H)}{\partial z}=\nabla(k\nabla T) \tag{4-1}$$

Where G_{mix} is the mixing mass flux, and $G_{mix}=\rho u_m$, in which u_m is the mixing flow velocity. Note that additional models for the mixing mass flux is needed, for which the high-fidelity CFD simulations using LES and uRANS can assist in the closure model developments. Special treatments are implemented for Eq. 4-1 in the SAM code because of its finite-element formulation while the flow mixing only occurs at the finite element boundary by definition.

A new governing equation (Eq. 4-2) is introduced for the mixing velocity. Note that its form is not originated from momentum conservation, but derived based on the energy conservation equation. The left side of the equation is the transport part (time derivative and advection terms), while the right side includes the diffusion term, resistance term, and the source terms. Recognizing three major contributions of the mixing flow, including local flow velocity, geometry, and the buoyancy effects, two parameters C_{gb} and C_{gv} are introduced in the mixing velocity equation.

$$\frac{\partial\rho u_m}{\partial t}+\frac{\partial(\rho u u_m)}{\partial z}=\mu\nabla^2 u_m+\frac{c_f f}{2D}\rho {u_m}^2+C_{gb}\beta\rho g\nabla T-\frac{c_f f}{2D}\rho(C_{gv}u)^2 \tag{4-2}$$

Where,

u_m is the mixing flow velocity;

u is the 1-D average flow velocity;

μ is the dynamic viscosity;

f is the friction coefficient using the average flow velocity u and the equivalent hydraulic diameter D;

c_f is the multiplier of the friction coefficient;

β is the thermal expansion coefficient of the fluid;

∇T is the temperature gradient;

C_{gb} is the coefficient for the buoyancy effects in the specific geometry; C_{gb} has a default value of 1 if it is not provided by users.

C_{gv} is the coefficient for the velocity effects in the specific geometry.

4.2 Verification Test Cases

The 1-D axial mixing model was tested for a generic simple 1-D channel flow, with geometry and boundary conditions specified in Table 4-1.

Table 4-1. Geometry and Boundary Conditions of a Single-phase Flow Test

Parameters	**Values**
Hydraulic Diameter (m)	0.02
Length (m)	1
Flow Area (m^2)	0.000314
Heat Source (W^3)	0
Inlet velocity (m/s)	0.1
Inlet temperature (K)	user-defined function

Two test cases are developed, i.e. the inlet temperature varied following two step changes or oscillated following a sinusoidal distribution.

$$T_{in}(t) = \begin{cases} 628, & t < 0 \\ 628 + 100t, & 0 \le t < 1 \\ 728, & 1 \le t < 11 \\ 728 - 100t, & 11 \le t < 12 \\ 628, & t \ge 12 \end{cases} \quad (4\text{-}3)$$

$$T_{in}(t) = 628 + 100sin\,(\pi t) \quad (4\text{-}4)$$

The inlet velocity is fixed, $u_{in}(t) = 0.5\ m/s$; and the initial pipe temperate is at 628 K. If the flow channel is unheated, the fluid temperature at any location *z* at ti*me t* can be linked with the inlet temperature (if fluid conduction and flow mixing are ignored):

$$T(z,t) = T(0, t - \frac{z}{u}) \quad (4\text{-}5)$$

The test cases listed in Table 4-2 and Table 4-3 were simulated with different modeling approaches and modeling parameters for the temperature step change test problem and the temperature oscillation problem, respectively. For the single 0D volume model, the 1-D channel is modeled as a 0-D volume and the inlet flow will mix with all the fluid in the channel instantaneously.

Table 4-2. Test Cases of Inlet Temperature Step Changes

Test Cases	Modeling Approaches	Modeling Parameters
1.1	Single 0D volume model	-
1.2	1D pipe model without axial mixing	-
1.3	1D pipe model with axial mixing	$C_{gb} = 1, C_{gv} = 0$
1.4	1D pipe model with axial mixing	$C_{gb} = 1, C_{gv} = 0.1$
1.5	1D pipe model with axial mixing	$C_{gb} = 1, C_{gv} = 1$
1.6	1D pipe model with axial mixing	$C_{gb} = 0, C_{gv} = 0.1$
1.7	1D pipe model with axial mixing	$C_{gb} = 0, C_{gv} = 1$

Table 4-3. Test Cases of Inlet Temperature Oscillation

Test Cases	Modeling Approaches	Modeling Parameters
2.1	Single 0D volume model	-
2.2	1D pipe model without axial mixing	-
2.3	1D pipe model with axial mixing	$C_{gb} = 1, C_{gv} = 0$
2.4	1D pipe model with axial mixing	$C_{gb} = 1, C_{gv} = 0.1$
2.5	1D pipe model with axial mixing	$C_{gb} = 1, C_{gv} = 1$
2.6	1D pipe model with axial mixing	$C_{gb} = 0, C_{gv} = 0.1$
2.7	1D pipe model with axial mixing	$C_{gb} = 0, C_{gv} = 1$

For Test Cases 1.1 through 1.5, the transient responses of the outlet temperature due to inlet temperature step changes are shown in Figure 4-1. The inlet temperature during the transient is also plotted as a reference. Clear differences were observed between the 0-D volume and 1D approaches. The outlet temperature responded simultaneously in the 0-D test case because of the perfect and instantaneous mixing modeling approach. A delay in outlet temperature response were observed in all 1-D test cases.

It is seen in Figure 4-1 that the axial mixing model only has minor effects on the transient responses of the outlet temperature. The differences between the axial mixing cases (Case 1.3-1.5) and the reference 1D case (Case 1.2) are small. This may be due to the temperature gradients were mostly zero in the channel expect narrow stratified regions. The buoyancy force was therefore zero except the narrow regions where temperature gradients were high. It is also observed the buoyancy effects are stronger than the velocity effects in this test problem. This is perhaps due to the small C_{gv} used in the simulations.

To investigate the effects of local velocity to flow mixing, two more test cases (Case 1.6 and 1.7) were simulated without the buoyancy effects activated ($C_{gb} = 0$). The transient responses of the outlet temperature are shown in Figure 4-2. It is confirmed that the velocity effects are very

small with smaller C_{gv}. It is also interesting to note that for Case 1.3 – 1.5, the outlet temperature is almost identical to the reference 1D case (Case 1.2) responding the second inlet temperature sharp change. During this time period, the buoyancy force is negative as the inlet temperature is lower than the pipe temperature. The strong buoyancy effects balanced the velocity effects, and the mixing velocity is almost equal to zero after the second inlet temperature change. When the buoyancy effects were de-activated in the simulation (Case 1.6 and 1.7), the effects of axial mixing model due to velocity effects were observed (in Figure 4-2) for the second temperature change as well.

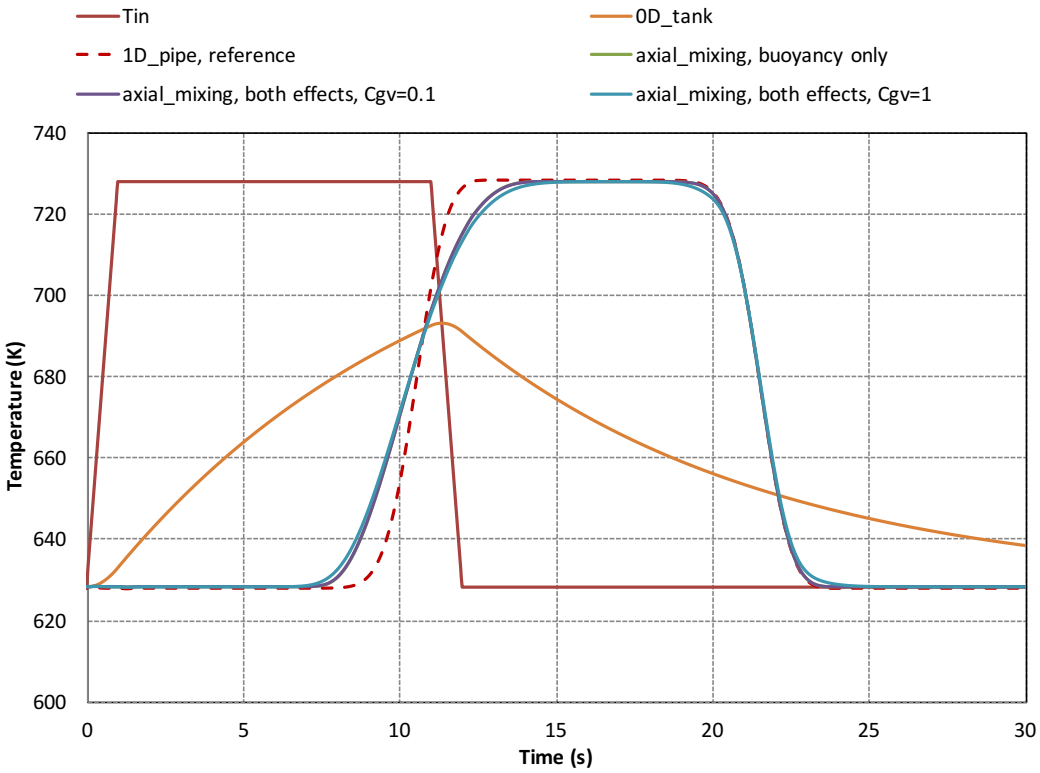

Figure 4-1. Outlet temperature response during the inlet temperature step change transient

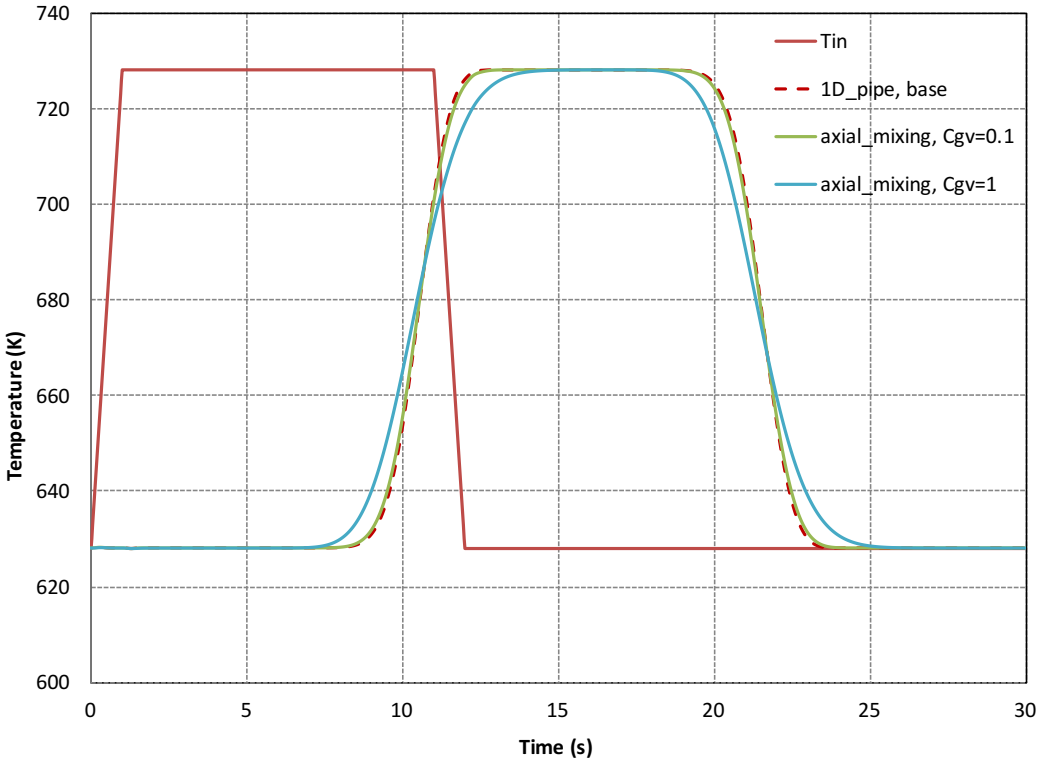

Figure 4-2. Outlet temperature response during the inlet temperature step change transient, buoyancy effects disabled

For Test Cases 2.1 through 2.5, the transient responses of the outlet temperature due to continuous changes of inlet temperature of a sinusoid wave function are shown in Figure 4-3. Again, it is observed that the outlet temperature responded simultaneously in the 0-D test case; while delayed effects were observed in all 1-D test cases. It is also shown the axial mixing model had stronger effects on the transient responses of the outlet temperature, comparing to the previous test problem. It is again observed the buoyancy effects are stronger than the velocity effects in this test problem, possibly due to the small C_{gv} used in the simulations.

To investigate the effects of local velocity to flow mixing, two more test cases (Case 2.6 and 2.7) were simulated without the buoyancy effects activated ($C_{gb} = 0$). The transient responses of the outlet temperature are shown in Figure 4-4. It is shown that the velocity effects are very strong, even with smaller C_{gv}. It is also interesting to note that for Case 1.6 – 1.7, the outlet temperature almost followed sinusoid functions with smaller oscillating magnitude, but not perfect sinusoid functions for Case 1.3-1.5. The buoyancy effects were positive or negative depending on the local temperature gradient, while the velocity effects were always positive. The buoyancy effects could be balanced by the velocity effects when the temperature gradients were positive (inlet temperature was decreasing so that lower temperature and heavier fluid were in the lower elevation) during the transient.

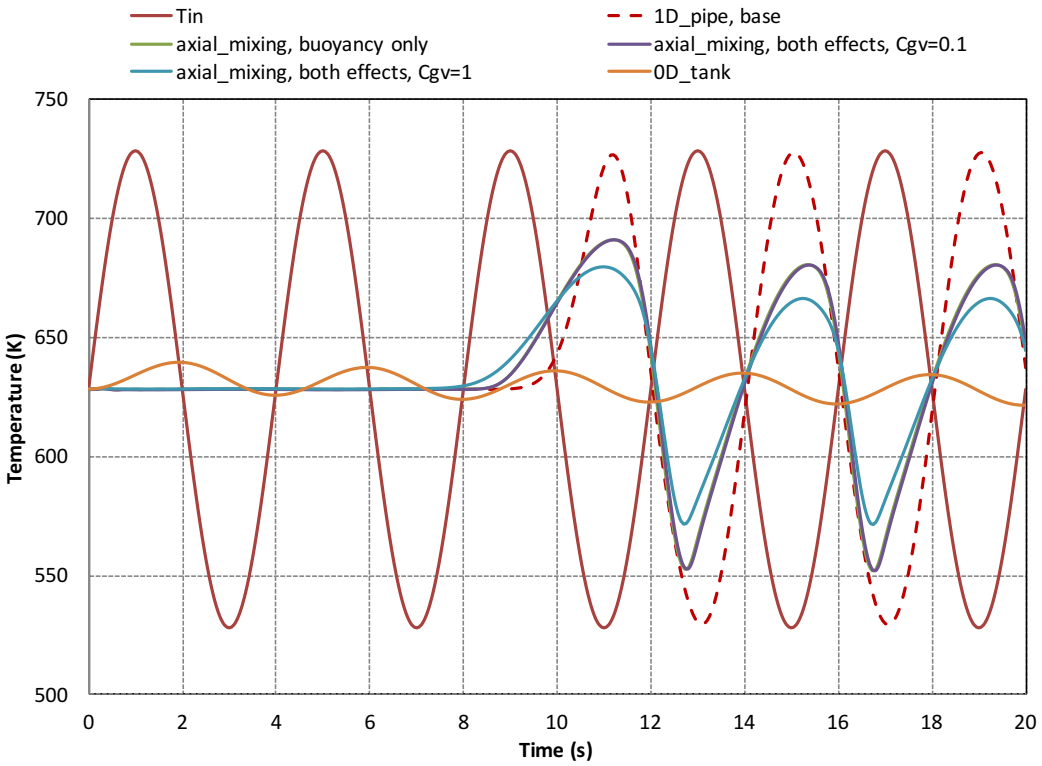

Figure 4-3. Outlet temperature response during the inlet temperature oscillation transient

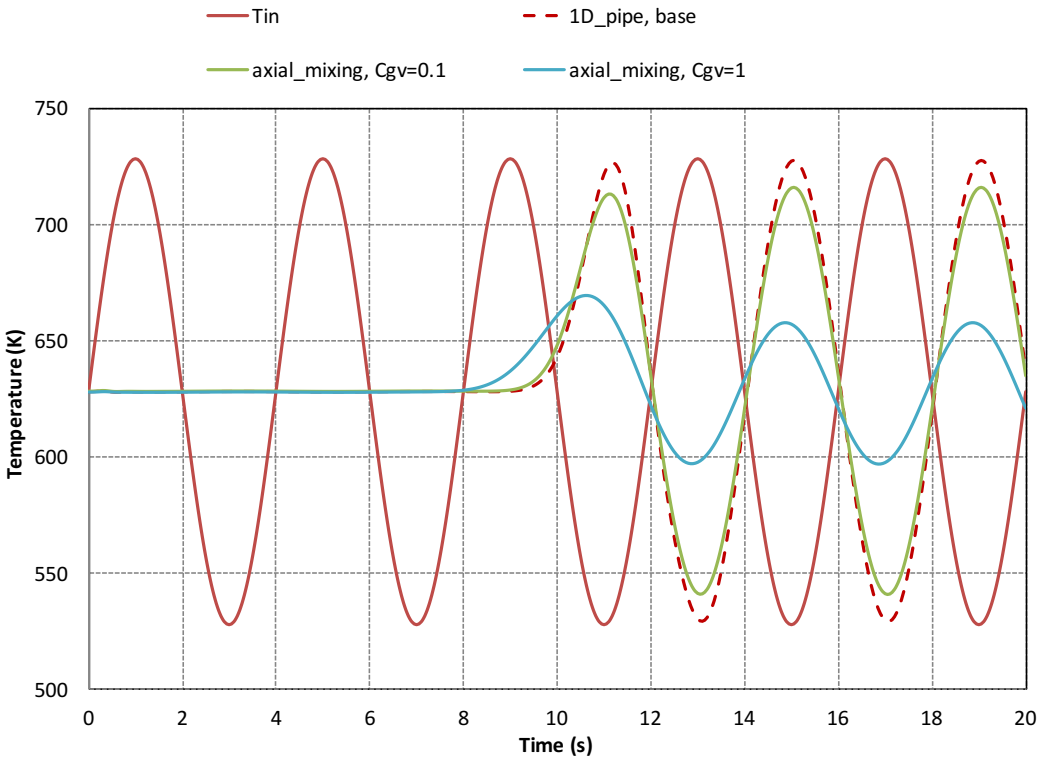

Figure 4-4. Outlet temperature response during the inlet temperature oscillation transient, buoyancy effects disabled

4.3 Demonstration Test Case of a Large Tank

To verify the applicability of the developed 1-D axial mixing model, a new test problem was developed based on the geometry and operating conditions of the upper plenum in the Advanced Burner Test Reactor (ABTR) design [32]. Transient CFD simulations of a stand-alone tank model are performed to provide the reference solutions.

The ABTR core outlet plenum is modeled as cylindrical tank, with parameters summarized in Table 4-4. The tank inlet conditions are also defined based on the representative conditions during a protected loss-of-flow transient, for which the core outlet plenum inlet flow rates and temperatures are provided as boundary conditions, shown in Figure 4-5.

Table 4-4. Geometric data of the Tank

Parameters	**Values**
Inlet Area (m^2)	0.1476
Flow Area (m^2)	5.975
Total Volume (m^3)	46.255
Liquid Level (m)	7.74
Tank Height (m)	10
Outlet Elevation (m)	4.1

4.3.1 CFD Simulation Results

uRANS (unsteady Reynolds-Averaged Navier-Stokes) -based simulations of the stand-alone tank case are being performed using the commercial CFD code STAR-CCM+ [33]. The CFD simulation results of the stand-alone tank model can be used as a reference to guide the development of the 0-D stratified volume model, 1-D mixing model, or other reduced-order models in system codes. A uniform inlet profile was used for both temperature and velocity at the tank inlet. The outlet boundary was extruded slightly in order to prevent potential reversed flow. Linear interpolation was used between the inlet boundary condition data points for transient boundary conditions. The tank is initially uniform in temperature. A slip wall condition is used at the top surface for simplicity.

Results for the tank outlet temperature, along with the inlet temperature and velocity, are provided in Figure 4-5. The inlet temperature drops sharply, causing cold sodium to be transported by the inlet jet to the upper portions of the tank, leading to a corresponding decrease in the outlet temperature. However, as the inlet velocity reduces, the cold mass of sodium sinks to the bottom of the tank, as seen in the remaining Figures (velocity at the outlet center plane, and temperature at the half-symmetry plane). This displaces the warmer sodium present around the periphery of the bottom of the tank and pushes it upward around the cylindrical wall. This is the reason for the brief increase in outlet temperature after the initial decrease.

After this point, the flow stratifies and the cold jet interacts with the stratified layer. As it pushes the warm sodium upward, waves are created in the layer, and eventually there are direct flow interactions between the jet and the outlet. These phenomena are the cause of the waviness in the outlet temperature profile after the large temperature drop. At around 400s the inlet velocity

reaches its steady low-flow condition, and combined with the increasing inlet temperature leads to a warm jet that rises to the top of the tank. This results in a slow and relatively steady heat-up of the tank.

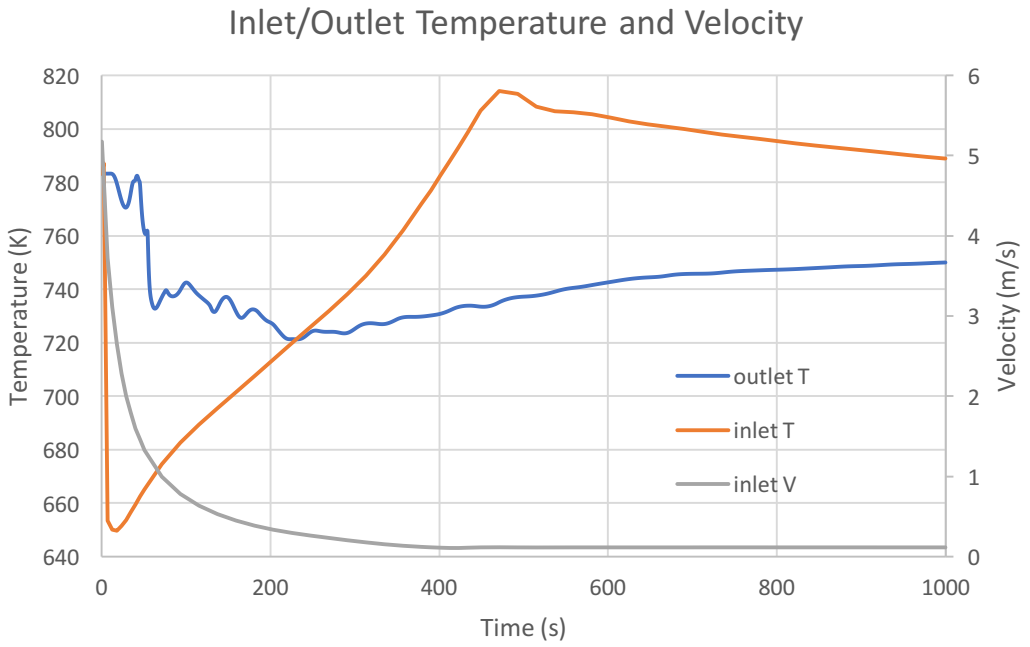

Figure 4-5. Inlet/Outlet Temperature and Velocity over the first 1000s of the transient.

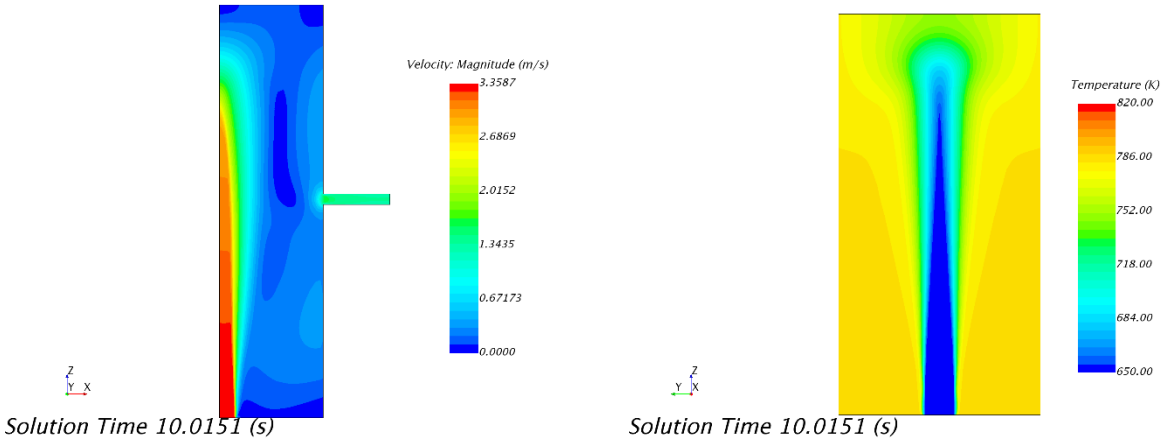

Figure 4-6. Velocity (left) and temperature (right) at t=10s.

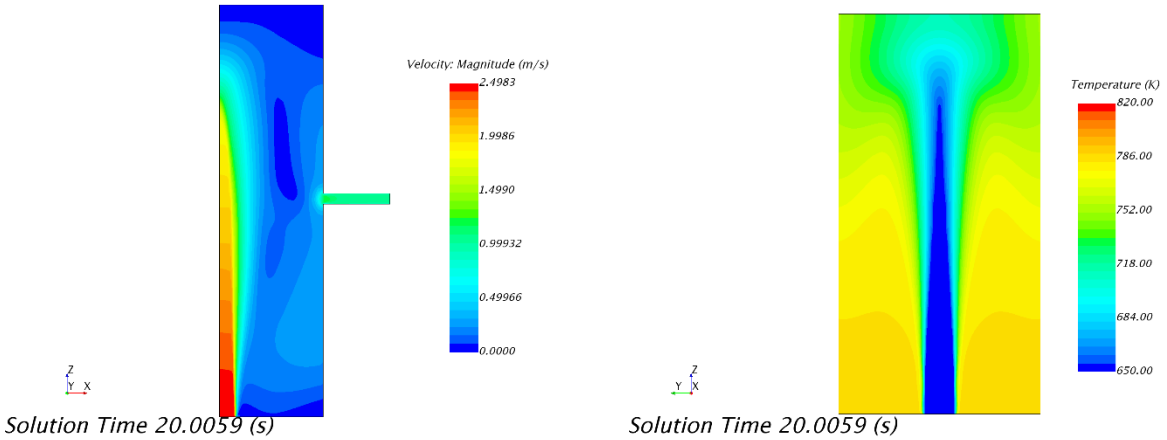

Figure 4-7. Velocity (left) and temperature (right) at t=20s.

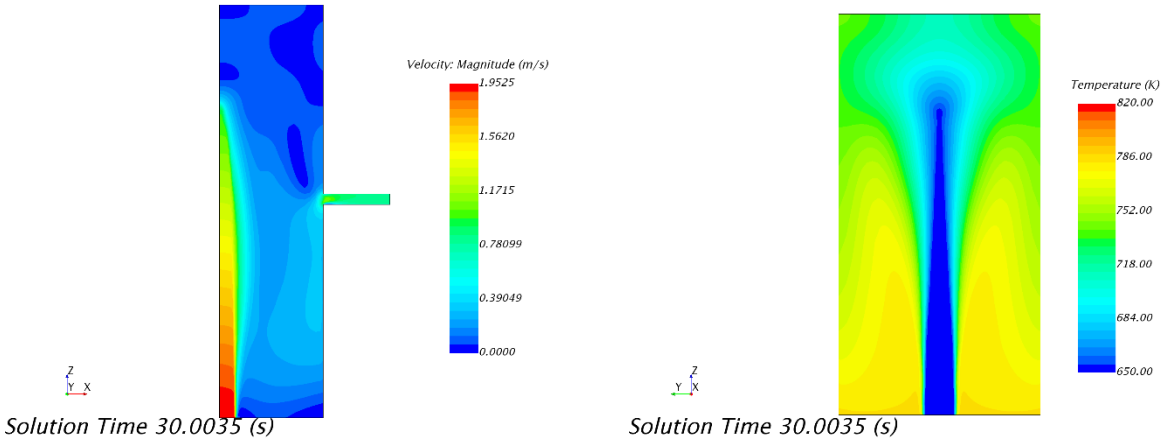

Figure 4-8. Velocity (left) and temperature (right) at t=30s.

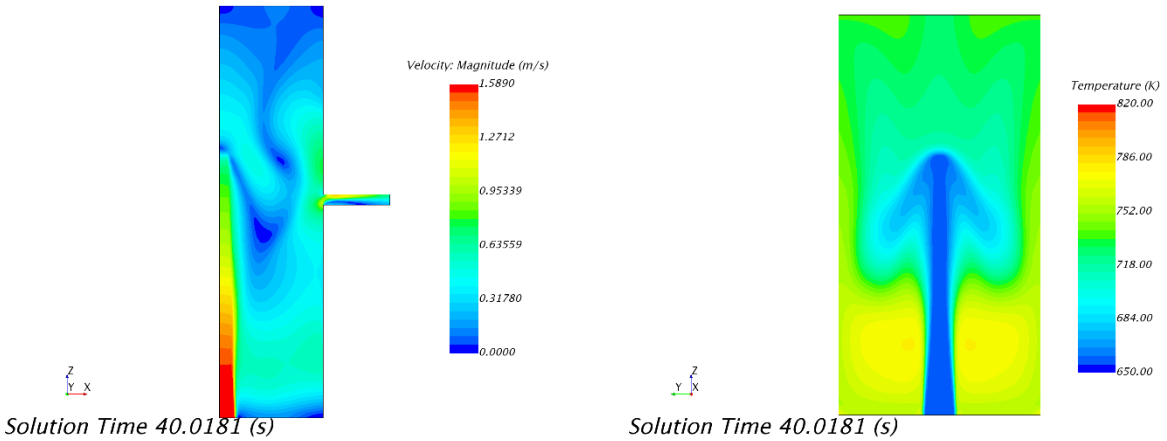

Figure 4-9. Velocity (left) and temperature (right) at t=40s.

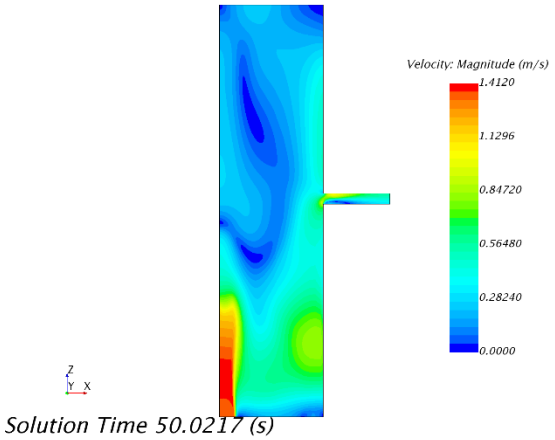

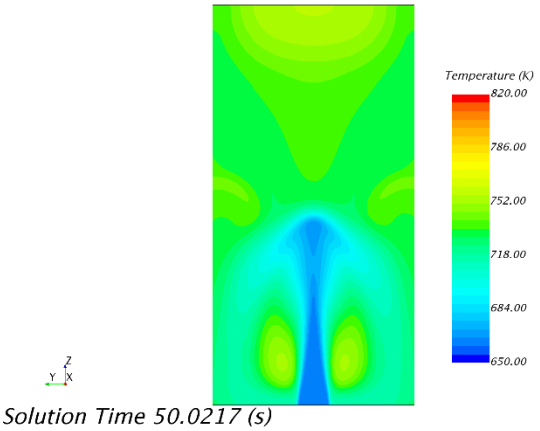

Figure 4-10. Velocity (left) and temperature (right) at t=50s.

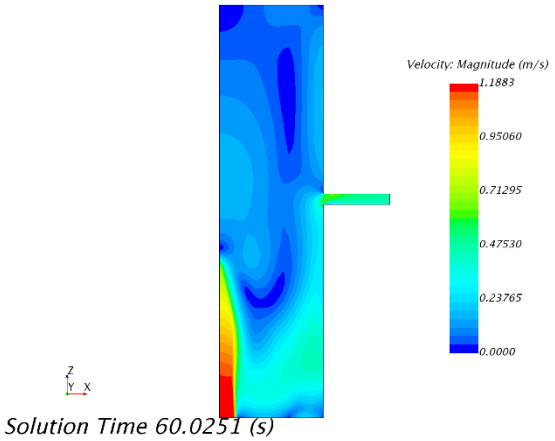

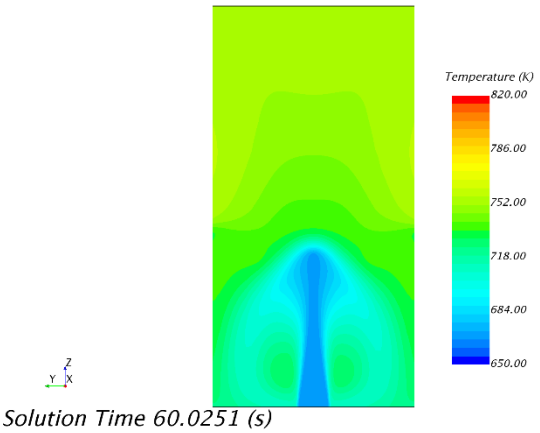

Figure 4-11. Velocity (left) and temperature (right) at t=60s.

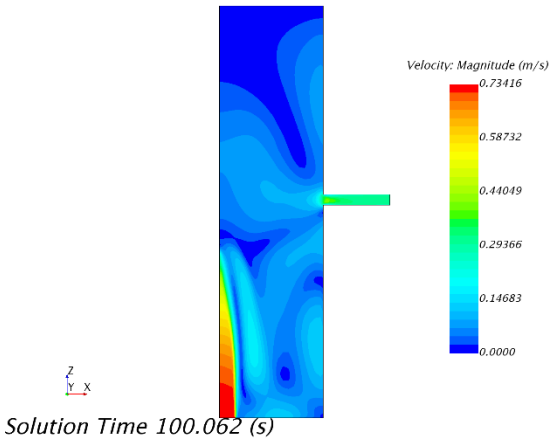

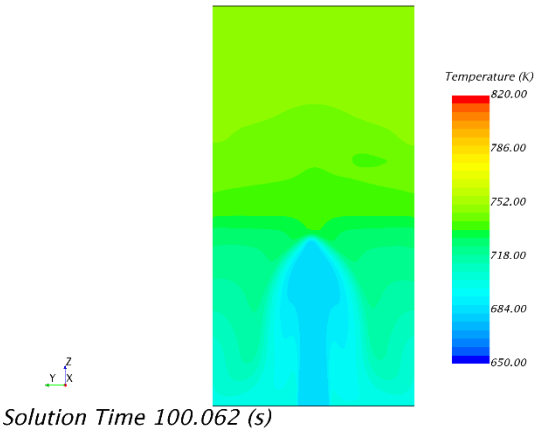

Figure 4-12. Velocity (left) and temperature (right) at t=100s.

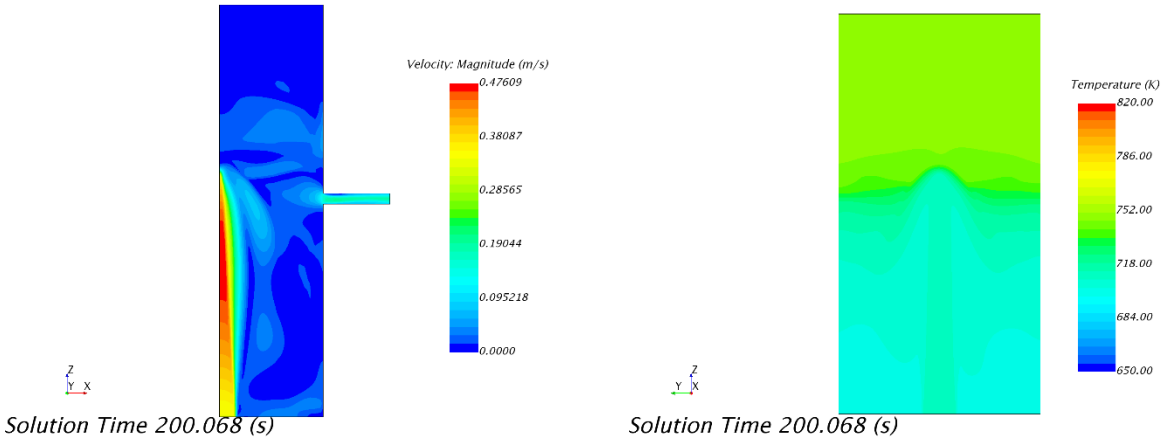

Figure 4-13. Velocity (left) and temperature (right) at t=200s.

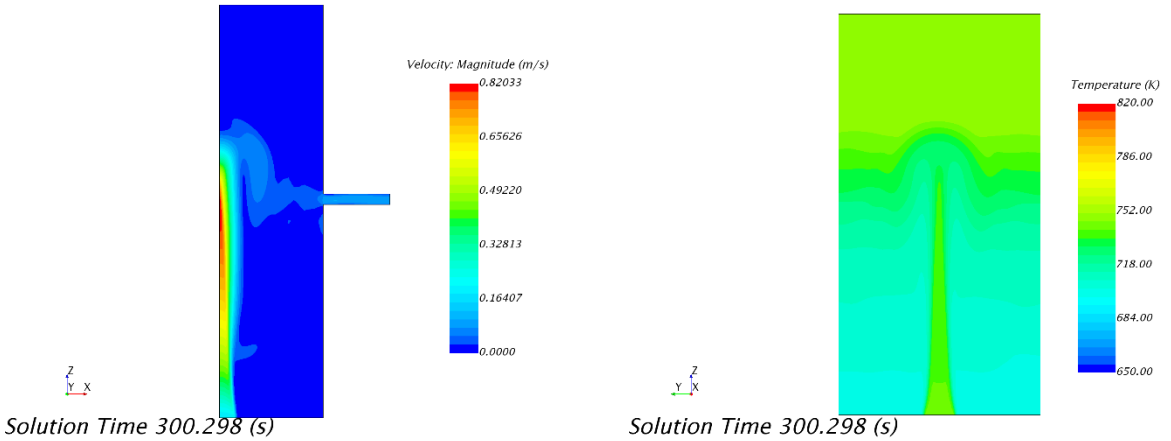

Figure 4-14. Velocity (left) and temperature (right) at t=300s.

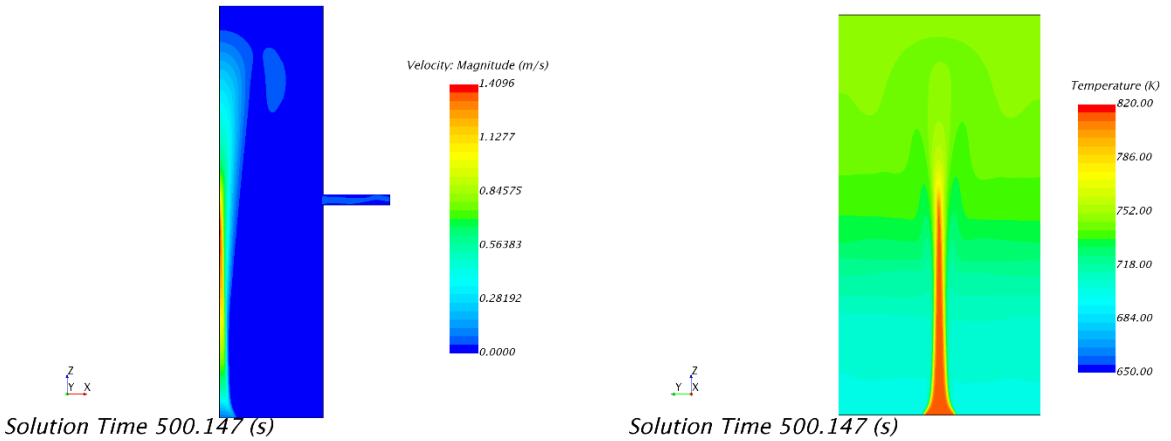

Figure 4-15. Velocity (left) and temperature (right) at t=500s.

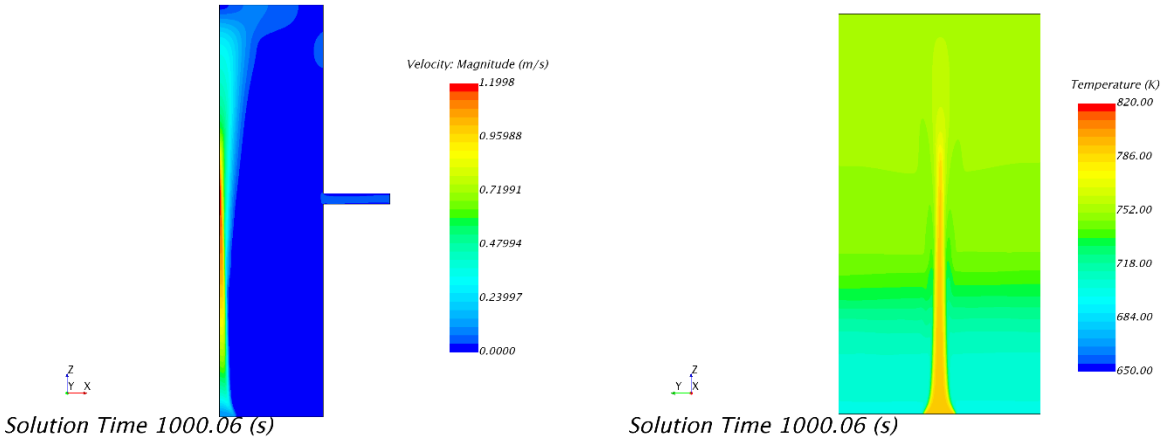

Figure 4-16. Velocity (left) and temperature (right) at t=1000s.

4.3.2 SAM Simulation Results

Similar to the test problem defined in Section 4.2, a number of test cases were simulated with different modeling strategies for the tank problem, listed in Table 4-5.

Table 4-5. Test Cases of Tank Demonstration Problem

Test Cases	Modeling Approaches
3.1	1D pipe model for the lower part of the tank, no upper part, no axial mixing
3.2	1D pipe model for the lower part of the tank, no upper part
3.3	1D pipe model for the lower part of the tank, single 0D volume model for the upper part
3.4	1D pipe model for the lower part of the tank, three 0D volume model for the upper part

The tank outlet temperature responses during the transient are shown in Figure 4-17 for various modeling approaches. With increasing complexities of the model, the SAM simulation results became closer to the reference CFD simulation results. For Case 3.1 and 3.2, the upper part of the tank (above the outlet pipe) was neglected in the models. It is seen that the outlet temperature responses were far away from the reference CFD simulation results. From Figure 4-6 to Figure 4-16, it is clearly observed the upper part was not stagnant and strongly participated the flow circulation and mixing in the tank. Once the upper tank is modeled, the simulation results are much closer to the CFD results. This preliminary demonstration case provides us some confidence that the 1D axial mixing model could simulate the macroscopic tank behavior during the transient with both accuracy and efficiency.

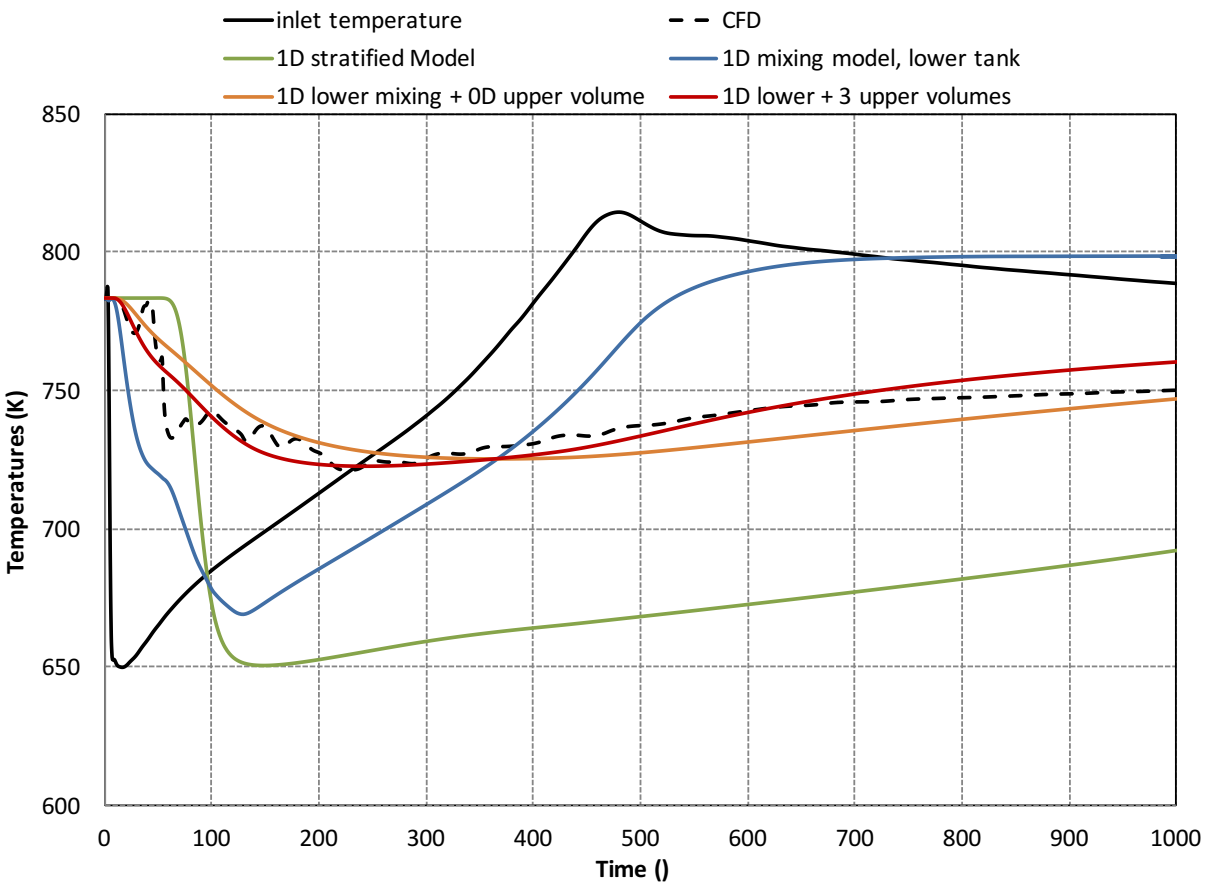

Figure 4-17. Outlet temperature response during the postulated loss-of-flow transient

5 Multi-Dimensional Fluid Model

While SAM is being developed as a system-level modeling and simulation tool, a three-dimensional flow module is also under development. While the 3D module will be useful for useful for a large number of reactor applications, the primary focus so far is to tackle the issue of thermal mixing and stratification modeling in large enclosures of reactor systems.

5.1 SAM 3-D Fluid Model and Current Status

The main objective of SAM 3-D fluid model is to provide a computationally efficient modeling capability to model the multi-dimensional flow and thermal stratification phenomena in large enclosures in nuclear systems. To achieve this, the key modeling approaches include:

1) Solving the full 3-D fluid equation;
2) Using only coarse computational meshes;
3) No turbulence modeling;
4) Developing closure models to account for the effects of turbulence and the use of coarse mesh in momentum and energy transport.

The transport equations for three-dimensional single-phase flow in a fluid domain can be described as a set of partial differential equations. The mass, momentum, and energy equations are closed by the equation of state of the fluid. It can be written in the conservative form (Equation 5-1) or in the non-conservative form (Equation 5-2).

$$
\begin{aligned}
&\frac{\partial \rho}{\partial t}+\frac{\partial(\rho u)}{\partial x}+\frac{\partial(\rho v)}{\partial y}+\frac{\partial(\rho w)}{\partial z}=0\\
&\frac{\partial \rho u}{\partial t}+\frac{\partial(\rho u u)}{\partial x}+\frac{\partial(\rho u v)}{\partial y}+\frac{\partial(\rho u w)}{\partial z}=-\frac{\partial p}{\partial x}+\nabla\cdot\vec{\tau}_x\\
&\frac{\partial \rho v}{\partial t}+\frac{\partial(\rho v u)}{\partial x}+\frac{\partial(\rho v v)}{\partial y}+\frac{\partial(\rho v w)}{\partial z}=-\frac{\partial p}{\partial y}+\nabla\cdot\vec{\tau}_y\\
&\frac{\partial \rho w}{\partial t}+\frac{\partial(\rho w u)}{\partial x}+\frac{\partial(\rho w v)}{\partial y}+\frac{\partial(\rho w w)}{\partial z}=-\frac{\partial p}{\partial z}+\nabla\cdot\vec{\tau}_z+\rho g\\
&\frac{\partial(\rho h)}{\partial t}+\frac{\partial(\rho u h)}{\partial x}+\frac{\partial(\rho v h)}{\partial y}+\frac{\partial(\rho w h)}{\partial z}=\nabla\left(k_{eff}\nabla T\right)+q_v'''\\
&\rho=\rho(p,T)
\end{aligned}
\qquad (5\text{-}1)
$$

In which, t: time; (x,y,z): the coordinate; ρ: coolant density; (u,v,w): velocity vector; g: the acceleration due to gravity; p: pressure; T: temperature; h: enthalpy; $\bar{\bar{\tau}}$: the shear stress and dependent on the velocity gradients and fluid properties, and for Newtonian fluid, $\tau_{ii}=2\mu\frac{\partial v_i}{\partial x_i}-\frac{2}{3}\mu\nabla\vec{v}$, and $\tau_{ij}=\tau_{ji}=\mu\left(\frac{\partial v_i}{\partial x_j}+\frac{\partial v_j}{\partial x_i}\right)$; k_{eff}: effective thermal conductivity, and $k_{eff}=k+\alpha$, which accounts for both normal thermal conductivity and additional diffusivity due to turbulence and the use of coarse mesh; q_v''': volumetric heat source.

$$\frac{\partial \rho}{\partial t}+\frac{\partial(\rho u)}{\partial x}+\frac{\partial(\rho v)}{\partial y}+\frac{\partial(\rho w)}{\partial z}=0$$

$$\rho\frac{\partial u}{\partial t}+\rho u\frac{\partial u}{\partial x}+\rho v\frac{\partial u}{\partial y}+\rho w\frac{\partial u}{\partial z}=-\frac{\partial p}{\partial x}+\nabla\cdot\vec{\tau}_x$$

$$\rho\frac{\partial v}{\partial t}+\rho u\frac{\partial v}{\partial x}+\rho v\frac{\partial v}{\partial y}+\rho w\frac{\partial v}{\partial z}=-\frac{\partial p}{\partial y}+\nabla\cdot\vec{\tau}_y \qquad (5\text{-}2)$$

$$\rho\frac{\partial w}{\partial t}+\rho u\frac{\partial w}{\partial x}+\rho v\frac{\partial w}{\partial y}+\rho w\frac{\partial w}{\partial z}=-\frac{\partial p}{\partial z}+\nabla\cdot\vec{\tau}_z+\rho g$$

$$\rho\frac{\partial h}{\partial t}+\rho u\frac{\partial h}{\partial x}+\rho v\frac{\partial h}{\partial y}+\rho w\frac{\partial h}{\partial z}=\nabla\left(k_{eff}\nabla T\right)+q'''_v$$

$$\rho=\rho(T)$$

If the incompressible approximation for the shear stress term is used:

$$\nabla\cdot\vec{\tau}_x=\mu\nabla^2 v_x=\mu\left(\frac{\partial^2 u}{\partial x^2}+\frac{\partial^2 u}{\partial y^2}+\frac{\partial^2 u}{\partial z^2}\right) \qquad (5\text{-}3)$$

Because of its dependence on the MOOSE framework, the SAM 3-D fluid model is also implemented in finite element method (FEM). It is well known that finite element analysis of incompressible flows requires stabilization to avoid potential numerical instabilities. The presence of advection terms (first order terms) in the governing equations can result in spurious node-to-node oscillations [34]. The Streamline-Upwind/Petrov-Galerkin (SUPG) and the Pressure-Stabilizing/Petrov-Galerkin (PSPG) scheme are implemented in SAM to resolve the numerical instability issues. In SAM, the weak forms of the PSPG/SUPG scheme are implemented as:

$$\left(\frac{\partial\rho}{\partial t}+\nabla\rho\vec{v},\ \psi\right)+\left(\rho\frac{\partial\vec{v}}{\partial t}+\rho\vec{v}\nabla\cdot\vec{v}+\nabla p-\nabla\cdot\bar{\bar{\tau}}-\rho\vec{f},\ \tau_{PSPG}\nabla\psi\right)=0$$

$$\left(\frac{\partial\rho\vec{v}}{\partial t}+\nabla\rho\vec{v}\vec{v}+\nabla p+-\nabla\cdot\bar{\bar{\tau}}-\rho\vec{f},\psi\right)$$

$$+\left(\rho\frac{\partial\vec{v}}{\partial t}+\rho\vec{v}\nabla\cdot\vec{v}+\nabla p-\nabla\cdot\bar{\bar{\tau}}-\rho\vec{f},\tau_{SUPG,m}\vec{v}\cdot\nabla\psi\right)=0 \qquad (5\text{-}4)$$

$$\left(\frac{\partial(\rho h)}{\partial t}+\nabla\cdot(\rho h\vec{v})-\nabla\left(k_{eff}\nabla T\right)-q''',\psi\right)$$

$$+\left(\rho\frac{\partial h}{\partial t}+\rho\vec{v}\nabla h-\nabla\left(k_{eff}\nabla T\right)-q''',\tau_{SUPG,e}\vec{v}\cdot\nabla\psi\right)=0$$

in which ψ is the test function; τ_{PSPG}, $\tau_{SUPG,m}$, and $\tau_{SUPG,e}$ are the stabilization parameters that weights the perturbations; and $(f,\psi)=\int_\Omega \psi\cdot f\, d\Omega$, is an expression of the volume integral.

Note that the regular residuals of all conservation equations are calculated based on the conservative form (Equation 5-1); while the residuals of the stabilization terms are calculated based on the non-conservative form (Equation 5-2). This formulation not only ensures the conservation laws, but also is easier to be implemented. A review of stabilized finite element

formulations for incompressible flow, including the SUPG and PSPG schemes, can be found in Reference [35].

Judicious selection of the stabilization parameters, τ_{PSPG} *and* τ_{SUPG}, plays a key role in determining the stability and accuracy of the formulations. The UGN-based stabilization parameters defined in Reference [36] are adapted in the SAM 3-D fluid model. The stabilization parameters are defined as:

$$\tau_{PSPG} = \left[\left(\frac{2}{\Delta t}\right)^2 + \left(\frac{2U}{h}\right)^2 + \left(\frac{4\nu}{h^2}\right)^2\right]^{-\frac{1}{2}}$$

$$\tau_{SUPG,m} = \left[\left(\frac{2}{\Delta t}\right)^2 + \left(\frac{2|\vec{v}|}{h}\right)^2 + \left(\frac{4\nu}{h^2}\right)^2\right]^{-1/2} \quad (5\text{-}5)$$

$$\tau_{SUPG,e} = \left[\left(\frac{2}{\Delta t}\right)^2 + \left(\frac{2|\vec{v}|}{h}\right)^2 + \left(\frac{4\alpha}{h^2}\right)^2\right]^{-1/2}$$

Where h is the element length scale; $\vec{v}$ is local velocity; Δt is the time step size; ν is the kinematic viscosity; α is the thermal diffusivity, $\alpha = \frac{k}{\rho C_p}$; and U is a global scaling velocity. If U were not defined in the simulation, the local velocity magnitude would be used.

The methodology presented above is very similar to the 1-D FEM model in SAM [19,20]. For computationally efficient modeling of the multi-dimensional flow in a coarse-grid CFD (CGCFD) approach, SAM does not implement any RANS-based turbulence models. Instead, it relies on closure models to close the equation system for the shear stress and the effective diffusivity terms. For laminar flow, the full set of fluid equations is solved, in which the shear stress terms are directly modeled.

$$\tau_{ii} = 2\mu\frac{\partial v_i}{\partial x_i} - \frac{2}{3}\mu\nabla\vec{v}$$

$$\tau_{ij} = \tau_{ji} = \mu\left(\frac{\partial v_i}{\partial x_j} + \frac{\partial v_j}{\partial x_i}\right) \quad (5\text{-}6)$$

For turbulent flow, additional closure models will be developed to account for the effects of turbulence and the use of coarse mesh in momentum and energy transport. The porous medium formulation has been implemented as an option in the SAM 3-D module, in which $\nabla\cdot\bar{\bar{\tau}} = \alpha|\vec{v}|\vec{v} + \beta\vec{v}$, α and β are porous resistance coefficients. A multi-scale modeling hierarchy is being pursued to develop practical predictive capability at the CGCFD level. High-resolution LES or u-RANS simulations will be leveraged to capture the fine details of the phenomena and to inform the needed closure model development.

The framework of a 3-D FEM flow model has been developed and implemented in SAM. To prevent the potential numerical instability issues, the SUPG and PSPG formulations have been implemented. Several verification and validation tests were performed, including lid-driven cavity flow, natural convection inside a cavity, and laminar flow in a channel of parallel plates. Based on

the comparisons with the analytical solutions and experimental results, it is demonstrated that the developed 3-D fluid model can perform very well for a range of laminar flow problems. For example, SAM simulation results of natural convection flow in a square cavity is shown in Figure 5-1. very good agreements were found between SAM simulation results and the experimental results [38]. More details on the SAM 3-D fluid model and the initial verification and validation results can be found an earlier paper [37].

This 3-D flow model is based on solving the primitive variables in the conservative form of the governing equations for incompressible but thermally expandable flows. Combined with the use of the JFNK solution method and high-order discretization schemes, this flow model has great potential for both efficient and accurate multi-dimensional flow simulations. Continued efforts have been focused on closure model developments based on high-fidelity CFD simulation results.

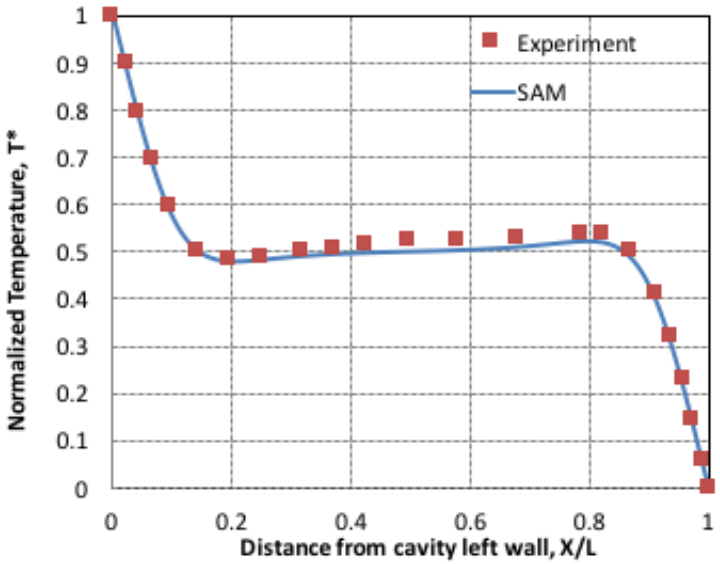

Figure 5-1.Comparison of normalized temperature distributions in a square cavity between SAM simulation and experimental results [37]

5.2 The data-driven turbulence model approach

A data-driven turbulence model approach has been pursued to leverage machine learning (ML) technique to establish a surrogate model in SAM to replace the turbulence model in traditional CFD code. The data-driven modeling approach has received increasing interest in the research community, including preliminary research in the nuclear thermal fluid applications [39,40,41].

For example, in normal RANS-based CFD code, the turbulence viscosity is a function of kinetic energy and dissipation rate, $\mu_t(k,\epsilon)$; but in the data-driven turbulence model to be implemented in SAM, the turbulence viscosity can be defined as a function of local system variables, $\mu_t(\nu,\rho,U,p,T,\nabla U,\nabla T,etc.)$. Since k and ϵ terms are deleted from conservation equation, the "computationally intensive" issue in traditional CFD simulations could be solved through using coarser mesh. Data-driven approach reveals the possibility of applying coarser mesh, but this remains to be tested.

5.2.1 *The framework of data-driven turbulence modeling*

The framework of data-driven turbulence modeling approach is depicted in Figure 5-2. It included four major steps:

1. Part of the full system domain is selected to perform high-fidelity CFD simulation, while the rest of the system will be modeled by a system code. CFD simulation results would be collected using CFD tool like OpenFOAM, StarCCM+, Nek5000, etc.
2. A machine learning surrogate model would be established based on training data from CFD simulations.
3. After the machine learning model been built with an acceptable error range, the model would be implemented into SAM with its conservation equations.
4. Perform the whole system simulation using the integrated code, which include both the 1-D flow module and the reduced-order 3-D flow module.

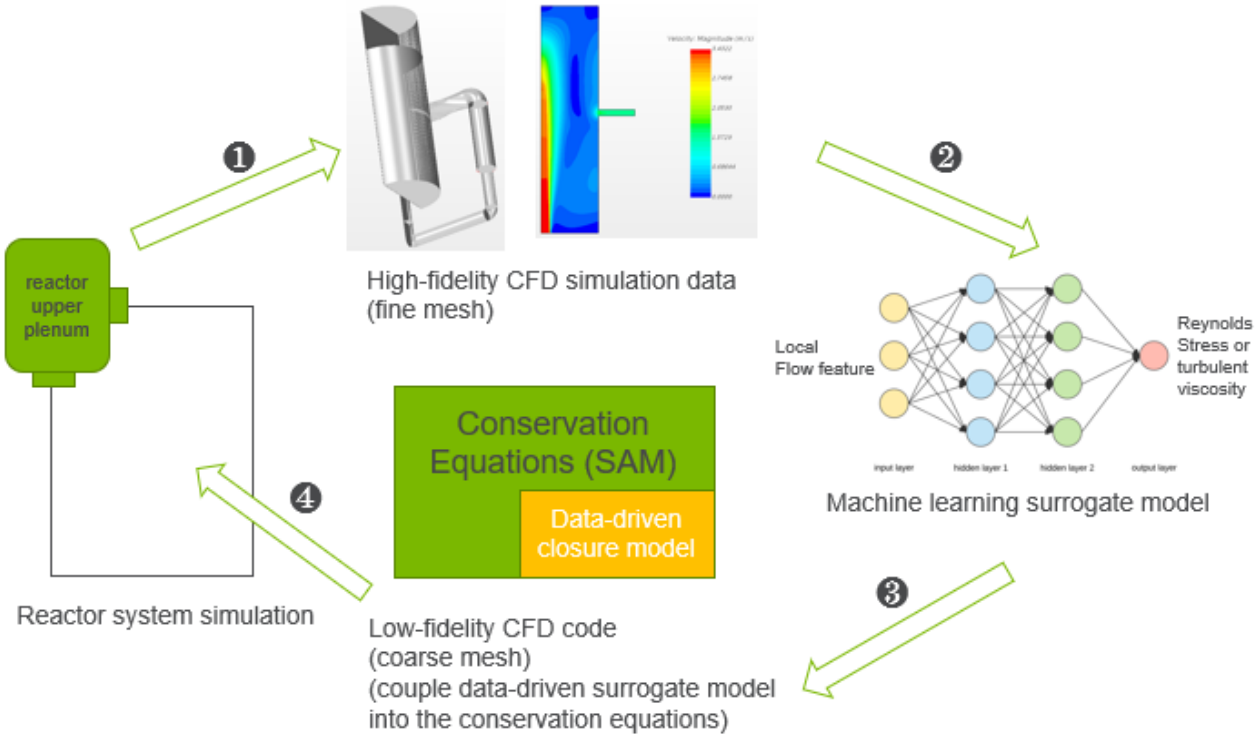

Figure 5-2.The framework of data-driven turbulence modeling problem

5.2.2 *Machine learning algorithm*

After reviewing three popular machine learning algorithms including neural network, Gaussian process regression, and decision tree/random forest, the neural network ML algorithm is selected in this work.

- For the neural network algorithm, the software implementation is readily available in some open source ML libraries such as TensorFlow and Pytorch. Additionally, after the ML model is trained, the testing and application of the ML model is very fast. However, it requires the

tuning of the hyper-parameters used in the training process which is a non-trivial work. The tuning of the hyper-parameters depends on experience and the specific applications.

- Gaussian process regression is easy to use, don't have many parameters to tune, and can provide prediction uncertainty range. However, the test process need to load all training data, so prediction is extremely slow! Prediction results would have large data density bias.
- Decision tree/Random forest method costs less training expense and shows better performance for multi-dimensional input training. However, the results have randomness, i.e., the prediction results can be different each time with the same input conditions. Therefore, it is not suitable for scientific modeling.

5.2.3 The workflow

The workflow of the data-driven approach could be depicted as below:

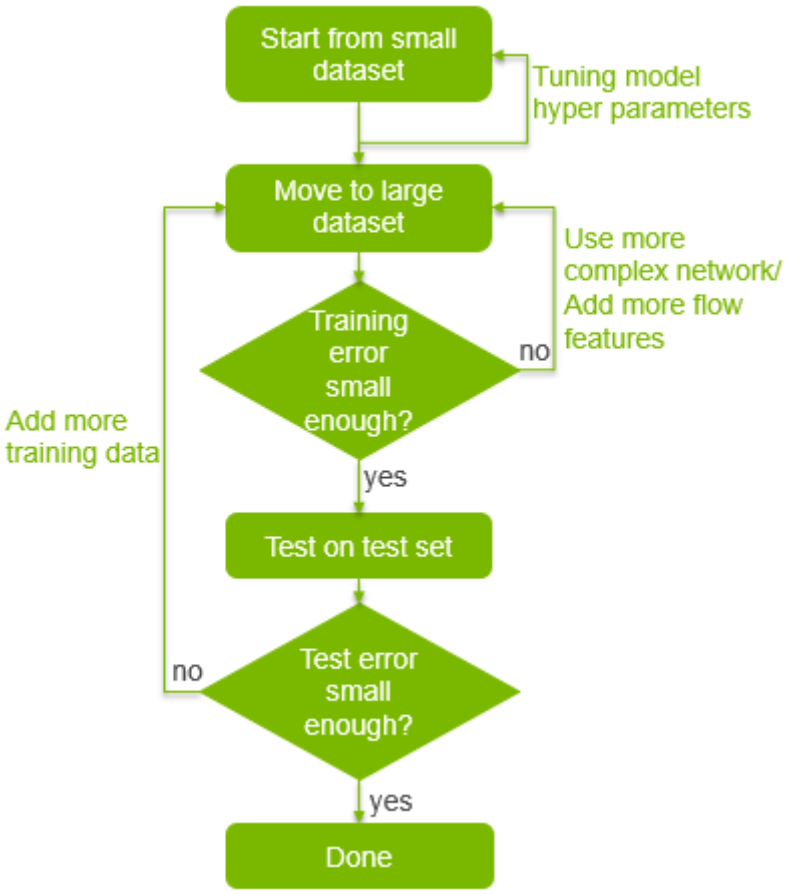

Figure 5-3. The workflow of the data-driven turbulence modeling approach

Firstly, the total data set is collected. The data amount can be very large if data of each point at each time step are collected. In order to deal with such large data, the model should be trained first on a small dataset to tune the hyperparameters in the neural network. After major hyper-parameters been tuned, the training data could then gradually be extended to larger datasets. During

this process, training and test should be done iteratively to finally obtain an appropriate setting. If the training error is not small enough, one should try to use more complex network; If test error is not small enough, one would consider adding more training data.

In most situation, a detailed experiment note table, such as an example shown in Figure 5-4, should be recorded to help decide what hyper-parameters are important and what you should do with the parameters (increase or decrease).

1	case id	training data	test data	GPU	flow feature	load model	Stopping Criteria	net structu	hidden_s	learning r	Ste
2		timestep100	timestep10	2*K20m	[b'Body Force[2]	FALSE	0.0216				
3		timestep200	timestep10	2*K20m	[b'Body Force[2]	FALSE	0.0224				
4		timestep300	timestep10	2*K20m	[b'Body Force[2]	FALSE	0.0247				
5		451,453	452	2*K20m	3,5,9,15,17,18,19,	FALSE	0.000156				
6	37	451,453	452	2*K20m	5,9,15,17,18,19,2	FALSE	0.0002	Net	1000		
7	38_1	451,453	452	2*K20m	5,9,15,17,18,19,2	FALSE	0.0002	deeperNet	1000		
8	39	451,453	452	2*K20m	5,9,15,17,18,19,2	FALSE	0.0002	Net	2000		
9	40_1	451,453	452	2*K20m	5,9,15,17,18,19,2	FALSE	0.0002	deeperNet	2000		
10	41	"400,410,420,430,440,450"	445	2*K20m	5,9,15,17,18,19,2	FALSE	0.0002	deeperNet	1000		
11	42	451,453	452	2*K20m	5,9,15,17,18,19,2	FALSE	0.0002	Net2(layer:	1000		
12	43	451,453	452	2*K20m	5,9,15,17,18,19,2	FALSE	0.0002	deeperNet	500		

Figure 5-4. Table of recorded test experiments

While in dealing with large data, a "random selection" method to choose hyper-parameters is not acceptable as it would take too much time. Instead, the "Control Variable" method is used, which test each parameter for three times with other parameters fixed. The trend of the three test results would assist in deciding an increase or decrease of the parameter. Although the "Control variable" method may miss some combination of parameters that is especially efficient, it cost way less time than a "random selection" method.

5.3 Case study of 3D thermal Stratification

5.3.1 Case introduction

The data-driven turbulence modeling approach is tested with a transient flow in a tank, as defined in Section 4.3 and also shown in Figure 5-5. The case aims to simulate a transient scenario mimicking the flow in the SFR upper plenum during a postulated loss-of-flow transient. The inlet flow rate gradually decreases to very low values, while inlet flow temperature decreases quickly immediately after the transient starts, then gradually increases to a new peak, and slowly decreases at the later stage of the transient.

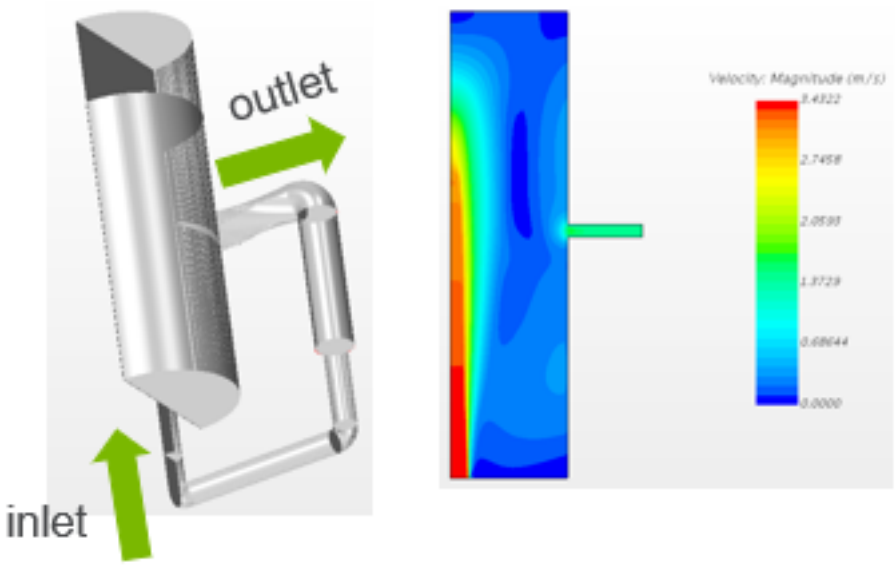

Figure 5-5. An illustrative picture of the test case geometry and velocity distribution before the transient

5.3.2 Model target and input

The main goal of this study is to train a surrogate model that could substitute traditional turbulence model to save computational expense. To achieve this goal, model input and target should be selected first. In this study we only use turbulence viscosity to represent Reynold stress so to reduce computation complexity and test the approach. The reason we used turbulence viscosity as model target in this work is because the training data of this 3D case is too large (3~5 TB). The currently available computational resource is not enough to support training large number of model targets. Therefore, only one major parameter, turbulence viscosity μ_t, is selected to represent all model targets.

The selected machine learning inputs (also called as flow features) include:

- Dynamic viscosity (Pa-s)
- Pressure (Pa)
- Temperature (K)
- Temperature Gradient (K/m)
- Velocity (m/s)
- Velocity Gradient (/s)
- Wall distance (m)

Current flow features are all basic variables in conservation equations. The time derivatives of temperature and velocity were not included initially, and are being included in the ongoing training process. Wall distance is added as near wall performance for turbulence is extremely different from other regions. We added the wall distance so that the model could apply different correlations for the near-wall region and other regions.

5.3.3 STEP1: tuning hyperparameters

Because the total data amount is too large. We started with 0.1% of the total data as training data to tune model hyperparameters. The 0.1% data could be randomly selected to reduce human bias. The parameters tuned from such data usually don't need to change much after this process.

In this work, the 0.1% data was selected from a small time range. In the CFD simulation, the total time steps are 5591. Partial data of the first 450 time-steps data are extracted as training data, while the rest of the data in the first 450 time-steps are used as testing data. The advantage here is to quickly test whether the model could make a good prediction for a short period. If it couldn't even make a good prediction for this short time period, it could mean some components of the model are incorrect, for example, selection of model input & target, network structure, optimization algorithm, etc.

The final tuned model hyper-parameters are as following:

1. Network structure: 5-layer network, 4 ReLU layer + 1 Tanh layer
2. Number of nodes in each layer: 1000
3. Batch normalization is turned off as they extremely slow down training speed (batch normalization could make train converge in fewer iterations, but each iteration would take more time to train. Overall it will delay training speed. If the computational resource is enough this option is suggested to be turned on.)
4. Learning rate: 0.0001
5. Learning rate decay: decay 0.3 after 200 iterations
6. Batch size: 2^18 = 262144
7. Number of workers = 4
8. Stopping Criteria: training error less than 0.00003
9. Optimization algorithm: ADAM (adaptive moment estimation) algorithm

5.3.4 STEP2: Extend the training dataset

When moving to a large dataset, one should follow the flowchart (Figure 5-3) to gradually increase the data amount. Because the whole data is too large to be used as training data, one would need to find the minimal set of training data. Currently, we use 4.2% of the total data as training data, such train could cost 2 weeks to reach 3e-5 training error with 1 node of GPU on the BLUES cluster at Argonne Laboratory Computing Resource Center (LCRC). Parallel training is also tested but the performance is not good (only 5% faster), so only 1 node of the GPU is used to train the model. With more time and computational resources, model data could be used, and better accuracy is expected.

5.3.5 Results

When dealing with a large dataset, this study follows the flowchart (**Error! Reference source not found.**) to gradually increase the data amount. Because the whole data is too large to be used as training data, only 4.2% of the total data are used as the training dataset.

Training data and test data

The training data are local data of each point in certain timesteps. The training timesteps are from timestep number listed below:

traindata="1,2,3,4,5,6,7,8,9,10,30,50,70,90,110,130,150,170,190,210,230,250,270,290,310,330,350,370,390,410,430,450,475,500,525,550,575,600,625,650,675,700,725,750,775,800,825,850,875,900,925,950,975,1000,1025,1050,1075,1100,1125,1150,1175,1200,1225,1250,1275,1300,1325,1350,1375,1400,1425,1450,1475,1500,1525,1550,1575,1600,1625,1650,1675,1700,1725,1750,1775,1800,1825,1850,1875,1900,1925,1950,1975,2000,2025,2050,2075,2100,2125,2150,2175,2200,2225,2250,2275,2300,2325,2350,2375,2400,2425,2450,2475,2500,2525,2550,2575,2600,2625,2650,2675,2700,2725,2750,2775,2800,2825,2850,2875,2900,2925,2950,2975,3000,3025,3050,3075,3100,3125,3150,3175,3200,3225,3250,3275,3300,3325,3350,3375,3400,3425,3450,3475,3500,3525,3550,3575,3600,3625,3650,3675,3700,3725,3750,3775,3800,3825,3850,3875,3900,3925,3950,3975,4000,4025,4050,4075,4100,4125,4150,4175,4200,4225,4250,4275,4300,4325,4350,4375,4400,4425,4450,4475,4500,4525,4550,4575,4600,4625,4650,4675,4700,4725,4750,4775,4800,4825,4850,4875,4900,4925,4950,4975,5000,5025,5050,5075,5100,5125,5150,5175,5200,5225,5250,5275,5300,5325,5350,5375,5400,5425,5450,5475,5500"

For the first 10 timesteps, all data are used. After that, we sample data every 20 timesteps. After 450 timesteps, we sample data every 25 timesteps until 5500 timesteps.

The test dataset is selected based on the “worst situation principle”, which means use the data that potentially has the worst prediction result, to test what the model would perform in the worst situations. For example, if training data is from timestep 50 and 70, then the data in timestep 60 is considered to potentially have the worst performance, and would be selected as test data. The test data selected in this study are listed below (as timestep numbers):

testdata="20,40,60,80,100,120,140,160,180,200,220,240,260,280,300,320,340,360,380,400,420,440,462,487,512,537,562,587,612,637,662,687,712,737,762,787,812,837,862,887,912,937,962,987,1012,1037,1062,1087,1112,1137,1162,1187,1212,1237,1262,1287,1312,1337,1362,1387,1412,1437,1462,1487,1512,1537,1562,1587,1612,1637,1662,1687,1712,1737,1762,1787,1812,1837,1862,1887,1912,1937,1962,1987,2012,2037,2062,2087,2112,2137,2162,2187,2212,2237,2262,2287,2312,2337,2362,2387,2412,2437,2462,2487,2512,2537,2562,2587,2612,2637,2662,2687,2712,2737,2762,2787,2812,2837,2862,2887,2912,2937,2962,2987,3012,3037,3062,3087,3112,3137,3162,3187,3212,3237,3262,3287,3312,3337,3362,3387,3412,3437,3462,3487,3512,3537,3562,3587,3612,3637,3662,3687,3712,3737,3762,3787,3812,3837,3862,3887,3912,3937,3962,3987,4012,4037,4062,4087,4112,4137,4162,4187,4212,4237,4262,4287,4312,4337,4362,4387,4412,4437,4462,4487,4512,4537,4562,4587,4612,4637,4662,4687,4712,4737,4762,4787,4812,4837,4862,4887,4912,4937,4962,4987,5012,5037,5062,5087,5112,5137,5162,5187,5212,5237,5262,5287,5312,5337,5362,5387,5412,5437,5462,5487,5512"

Prediction accuracy

The surrogate model is evaluated by prediction accuracy, which is defined here by the portion of test data that satisfy the required test error divided by the total amount of test data. The test error is the difference between the ML model predictions and the CFD simulation results.

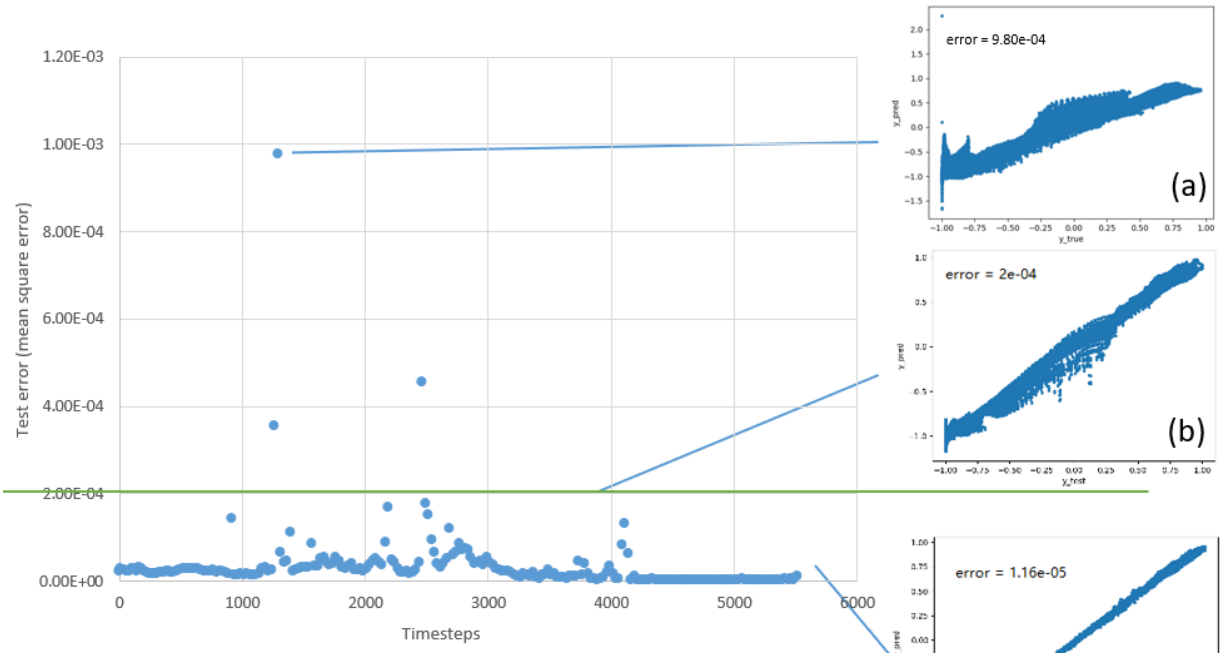

Acceptable error range	Prediction accuracy
2e-04	98.68%
5e-05	86.34%
1.16e-05	31.72%

Figure 5-6. Prediction accuracy for the different acceptable error range

In Figure 5-6, each point in the left picture represents the mean square error of all the data in that time step. On the right-hand side, each of the 3 pictures illustrates how the test errors correlated with the actual performance between the "true" turbulence viscosity (from CFD results) and model predicted turbulence viscosity. For Figure 5-6(a,b,c), the x-axis is the turbulence viscosity from CFD results and the y-axis is ML model predicted turbulence viscosity. As can be seen, if the test error is reduced to 1.16e-5, the actual correlation, shown in Figure 5-6c, is much better than those in Figure 5-6(a) and Figure 5-6(b). So, the less test error, the better the model.

Acceptable error range is another important term. It is defined here as the acceptable error that could still allow CFD calculation to perform without diverging or running into the wrong solution. If the acceptable error range is 2e-4, which is the green line in Figure 5-6, then nearly all the points are below this value, the prediction accuracy is 98.68%. If the better model is required, then the acceptable error range should be reduced accordingly. When acceptable error range is equal to 5e-5, the prediction accuracy is 86.34%; when the acceptable error range is equal to 1.16e-5, the prediction accuracy is 31.72%.

It could be seen from Figure 5-6 that, after 4000 timesteps, our prediction result becomes much better. This may relate to the fact that the flow becomes more and more steady. Time derivative terms may need to be added into the model input/flow feature. In the first 450 iterations, we use 5% data as training data; In the following 5000 iterations, we use 4% data as training data. So, the data sample rate is very similar, but the performance differs a lot, especially in 1000~4200 timesteps, when flow dynamics was very complex due to various contributing phenomena.

A similar study has also been performed with less training data to test the impacts the training data amount to the final prediction accuracy. As can be seen in Table 5-1, increasing training data amount from 2.4% to 4.2% of total data highly improved model prediction accuracy. It is believed that with more data been used as training data, higher prediction accuracy could be achieved.

Table 5-1. Prediction accuracy of models trained by different amount of training data

Acceptable error range	Prediction accuracy (use 2.4% data as training data)	Prediction accuracy (use 4.2% data as training data)
2e-04	91.06%	98.68%
5e-05	59.54%	86.34%
1.16e-05	21.14%	31.72%

5.3.6 Notes on computing resources

The current limitation in this work or in any other data-intensity ML application is mainly the available computing resources (mainly GPU resources).

1. The data amount is 3TB in binary format from all processed CFD results. Data is large because we collect data of each point in each time step. Such large data requires high computational resources.
2. Currently major machine learning frameworks or libraries are all developed for GPU. Some have CPU version but only for the very simple cases.
3. The Parallel GPU computing technology is still immature. The Parallel GPU technique were tried with the Argonne LCRC/BLUES and ALCF/Cooley clusters. But the performance was very bad, i.e., the calculation speed for 12 GPUs is only 7% faster than 2GPUs on 1 motherboard.

5.4 Summary and Future Works

A data-driven turbulence or closure model development framework has been developed for SAM 3D flow module. The accuracy of it remains to be improved. To increase model accuracy, sufficient computational resource will need to be acquired or secured. One solution is to switch to 2D cases so that the training would cost less time. Also, time derivative terms of temperature and velocity are expected to be added into flow feature, potentially increasing the model accuracy at a higher level. After increasing model accuracy into an acceptable level, the next step would be

implementing the model into SAM, which may bring additional challenge as the performance of the ML-based model will need to be further examined on coarse meshes.

ACKNOWLEDGMENTS

This work is supported by U.S. DOE Office of Nuclear Energy's Nuclear Energy Advanced Modeling and Simulation (NEAMS) program. We gratefully acknowledge use of the Blues and Bebop clusters in the Laboratory Computing Resource Center and the Eddy cluster in the Nuclear Engineering Division at Argonne National Laboratory.

Reference:

1. S. Moriya, N. Tanaka, N. Katano and A. Wada, "Effects of Reynolds Number and Richardson Number on Thermal Stratification in Hot Plenum," *Nuclear Engineering and Design*, **Vol. 99**, 441-451, (1987).
2. Y. Ieda, I. Maekawa, T. Muramatsu and S. Nakanishi, "Experimental and Analytical Studies of the Thermal Stratification Phenomenon in the Outlet Plenum of Fast Breeder Reactors," *Nuclear Engineering and Design*, **Vol. 120**, 403-414, (1990).
3. Auban, et. al., "Investigation of Large-scale Gas Mixing and Stratification Phenomena related to LWR Containment Studies in the PANDA Facility," *Nuclear Engineering and Design*, **Vol. 237**, pp. 409-419 (2007).
4. M. Andreani, A. Badillo, and R. Kapulla, "Synthesis of the OECD/NEA-PSI CFD benchmark exercise," *Nuclear Engineering and Design* **299**, 59-80, (2016).
5. H. Zhao and P. Peterson, "An Overview of Modeling Methods for Thermal Mixing and Stratification in Large Enclosures for Reactor Safety Analysis," *Proceedings of NUTHOS-8*, Shanghai, China, October 10-14, (2010).
6. T.H. Fanning, (Ed.), The SAS4A/SASSYS-1 Safety Analysis Code System, ANL/NE-12/4. Argonne National Laboratory, 2012.
7. INL, RELAP5-3D Code Manual Volume I: Code Structure, Systems Models, and Solution Methods, INEEL-EXT-98-00834 Rev. 2.0, (2002).
8. M. Robert, M. Farvacque, M. Parent, and B. Faydide, "CATHARE 2 V2.5: A Fully Validated CATHARE Version for Various Applications," *Proceedings of NURETH-10*, Seoul, Republic of Korea, October 5–9, 2003.
9. US Nuclear Regulatory Commission, MELCOR Computer Code Manuals, NUREG/CR-6119, Vol. 2, Rev. 3, SAND 2005-5713 (2005).
10. P. F. Peterson, "Scaling and analysis of mixing in large stratified volumes," *International Journal of Heat and Mass Transfer*, **Vol. 37**, no. 1, pp. 97–106, 1994.
11. P. F. Peterson and R. Gamble, "Scaling for forced-convection augmentation of heat and mass transfer in large enclosures by injected jets," *Transactions of the American Nuclear Society*, **Vol. 78**, pp. 265–266, 1998.
12. H. Zhao, Computation of Mixing in Large Stably Stratified Enclosures, Ph.D. dissertation, University of California, Berkeley (2003).
13. S. Kuhn, H. K. Kang, and P. F. Peterson, "Study of mixing and augmentation of natural convection heat transfer by a forced jet in a large enclosure," *Journal of Heat Transfer*, **Vol. 124**, no. 4, pp. 660–666, 2002.
14. H. Zhao, L. Zou, H. Zhang, "Simulation of thermal stratification in BWR suppression pools with one dimensional modeling method," *Annals of Nuclear Energy*, **63**, 533-540, (2014).

15. A. Kraus and R. Hu, "CFD Analysis of Upper Plenum Flow for a Sodium-Cooled Small Modular Reactor," *Proceedings of NURETH-16*, Chicago, IL, US, August 30 - September 4, 2015.
16. T. H. Fanning and J. W. Thomas, "Integration of CFD into systems analysis codes for modeling thermal stratification during SFR transients," *Proceedings of NURETH-14,* Toronto, ON, Canada, September 25-30, 2011.
17. R. Hu, J. W. Thomas, and T. H. Fanning, "Strategy for Multi-Scale Single-Phase Flow Coupling," ANL/NE-13/4, Argonne National Laboratory, March 2013.
18. R. Hu, SAM Theory Manual, Argonne National Laboratory, ANL/NE-17/4, March 2017.
19. R. Hu, "A fully-implicit high-order system thermal-hydraulics model for advanced non-LWR safety analyses," *Annals of Nuclear Energy*, **Vol. 101**, 174–181, (2017).
20. R. Hu, "An Advanced One-Dimensional Finite Element Model for Incompressible Thermally Expandable Flow", *Nuclear Technology*, **Vol. 190**, No. 3, 313-322, (2015).
21. D. Gaston, C. Newman, G. Hansen, and D. Lebrun-Grandi´e, "MOOSE: A parallel computational framework for coupled systems of nonlinear equations," *Nuclear Engineering and Design*, **vol. 239**, pp. 1768–1778, (2009).
22. Kirk B. S., Peterson J. W., Stogner R. H., et al., 2006. "libMesh: A C++ Library for Parallel Adaptive Mesh Refinement/Coarsening Simulations," Engineering with Computers, 22(3-4): 237-254.
23. Balay S., Brown J., et al, 2017. PETSc Web page, http://www.mcs.anl.gov/petsc.
24. D. A. Knoll and D. E. Keyes, "Jacobian-free Newton-Krylov Methods: A Survey of Approaches and Applications," *Journal of Computational Physics*, **Vol. 193**, pp.357–397 (2004).
25. Berry R. A., Peterson J. W., Zhang H., et al., 2015. "RELAP-7 Theory Manual," INL/EXT-14-31366, Idaho National Laboratory.
26. R. Hu, J. W. Thomas, E. Munkhzul, T. H. Fanning, "Coupled System and CFD Code Simulation of Thermal Stratification in SFR Protected Loss-Of-Flow Transients," *Proceedings of ICAPP 2014*, Charlotte, NC, April 6-9, 2014.
27. T.H. Fanning and R. Hu, "Coupling the System Analysis Module with SAS4A/SASSYS-1," ANL/NE-16/22, Argonne National Laboratory, September 2016.
28. R. Martineau, D. Andrs, J. Hansel, C. Permann, M. Bernard, R. Johns, R. Hu, J. Wolf, H. Zhang, R. Szilard, "Extending the Capability of Nuclear Plant Systems Analysis with Advanced Tightly-Coupled Nuclear Fuels Performance", 2018 American Nuclear Society Annual Meeting, Philadelphia PA, June 17 - 21, 2018.
29. K. Ahmed, R. Scarlat, R. Hu, "Benchmark Simulation of Natural Circulation Cooling System with Salt Working Fluid Using SAM," *Proceedings of NURETH-17*, Xi'an China, September 3-8, 2017.
30. G. Zhang and R. Hu, "Development of MSR Transient Safety Analysis Capability in SAM", 2018 American Nuclear Society Annual Meeting, Philadelphia PA, June 17 - 21, 2018.
31. R. Hu and T. Sumner, "Benchmark Simulations of the Thermal-Hydraulic Responses during EBR-II Inherent Safety Tests using SAM", *Proceedings of ICAPP'16*, San Francisco CA, April 17-20, 2016.
32. Y. I. Chang, P. J. Finck, C. Grandy, et al., "Advanced Burner Test Reactor Preconceptual Design Report," ANL-ABR-1 (ANL-AFCI-173), Argonne National Laboratory, September 2006.

33. CD-adapco, “STAR-CCM+ 10.06 Manual,” N.Y., (2015).
34. A.N. Brooks, T.J.R. Hughes, “Streamline upwind/Petrov-Galerkin formulations for convection dominated flows with particular emphasis on the incompressible Navier-Stokes equations,” *Comp. Methods Appl. Mech. Engrg.*, **32**, 199 – 259, (1982).
35. T.E. Tezduyar, "Stabilized Finite Element Formulations for Incompressible Flow Computations," *Advances in Applied Mechanics*, **Vol. 28**, 1-44, (1992).
36. T. Tezduyar and Sunil Sathe, “Stabilization Parameters in SUPG and PSPG Formulations,” *Journal of Computational and Applied Mechanics*, **Vol. 4**, No. 1, pp. 71-88, (2003).
37. R. Hu, “Development of a Reduced-Order Three-Dimensional Flow Model for Thermal Mixing and Stratification Simulation during Reactor Transients,” Proceedings of NURETH-17, Xi’an China, September 3-8, 2017.
38. R. J. Krane and J. Jessee. "Some detailed field measurements for a natural convection flow in a vertical square enclosure." *1st ASME-JSME thermal engineering joint conference*. Vol. 1. ASME New York, 1983.
39. Y. Liu, N. Dinh, Y. Sato, B. Niceno, "Data-driven modeling for boiling heat transfer: using deep neural networks and high-fidelity simulation results," *Applied Thermal Engineering*, Volume 144, 305-320, 2018.
40. C.W. Chang, N. T Dinh, "Classification of Machine Learning Frameworks for Data-Driven Thermal Fluid Models," arXiv preprint arXiv:1801.06621, 2018.
41. H. Bao, N. Dinh, J. Lane, R. Youngblood, "Study of Data-Driven Mesh-Model Optimization in System Thermal-Hydraulic Simulation, " 2018 ANS Annual Meeting, Philadelphia PA, June 17 - 21, 2018.

Nuclear Science and Engineering Division
Argonne National Laboratory
9700 South Cass Avenue, Bldg. 208
Argonne, IL 60439

www.anl.gov

Argonne National Laboratory is a U.S. Department of Energy laboratory managed by UChicago Argonne, LLC